



Design and synthesis of newer 1,3,4-oxadiazole and 1,2,4-triazole based Topsentin analogues as anti-proliferative agent targeting tubulin

Fatima Naaz^a, Faiz Ahmad^b, Bilal Ahmad Lone^b, Yuba Raj Pokharel^b, Neeraj Kumar Fuloria^c, Shivkanya Fuloria^c, Manickam Ravichandran^d, Lalitha Pattabhiraman^e, Syed Shafi^{f,*}, M. Shahar Yar^{a,*}

^a Department of Pharmaceutical Chemistry, School of Pharmaceutical Education and Research, Jamia Hamdard, New Delhi, India

^b Faculty of Life Sciences and Biology, South Asian University, New Delhi 110021, India

^c Faculty of Pharmacy, AIMST University, Semeling Campus, Jalan Bedong-Semeling, Bedong, Kedah Darul Aman 08100, Malaysia

^d Faculty of Applied Science, AIMST University, Semeling Campus, Jalan Bedong-Semeling, Bedong, Kedah Darul Aman 08100, Malaysia

^e Faculty of Medical Sciences, AIMST University, Semeling Campus, Jalan Bedong-Semeling, Bedong, Kedah Darul Aman 08100, Malaysia

^f Department of Chemistry, School of Chemical and Life Science, Jamia Hamdard, New Delhi, India

ARTICLE INFO

Keywords:

1,3,4-oxadiazole
1,2,4-Triazole
Topsentin
Anti-proliferation
Colchicine
Tubulin
Cancer cell line

ABSTRACT

A set of two series of 1,3,4-oxadiazole (**11a-n**) and 1,2,4-Triazole (**12a, c, e, g, h, j-n**) based topsentin analogues were prepared by replacing imizadole moiety of topsentin through a multistep synthesis starting from indole. All the compounds synthesized were submitted for single dose (10 μM) screening against a NCI panel of 60-human cancer cell lines. Among all cancer cell lines, colon (HCC-2998) and Breast (MCF-7, T-47D) cancer cell lines were found to be more susceptible for this class of compounds. Among the compounds tested, compounds **11a**, **11d**, **11f**, **12e** and **12h**, were exhibited good anti-proliferative activity against various cancer cell lines. Compounds **11d**, **12e** and **12h** demonstrated better activity with IC_{50} 2.42 μM , 3.06 μM , and 3.30 μM respectively against MCF-7 human cancer cell line than that of the standard drug doxorubicin IC_{50} 6.31 μM . Furthermore, **11d** induced cell cycle arrest at G0/G1 phase and also disrupted mitochondrial membrane potential with reducing cell migration potential of MCF-7 cells in dose dependent manner. *In vitro* microtubule polymerization assays found that compound **11d** disrupt tubulin dynamics by inhibiting tubulin polymerization with IC_{50} 3.89 μM compared with standard nocodazole (IC_{50} 2.49 μM). *In silico* docking studies represented that **11d** was binding at colchicine binding site of β -tubulin. Compound **11d** emerged as lead molecule from the library of compounds tested and this may serve as a template for further drug discovery.

1. Introduction

Cancer comprises of more than 200 diseases which are illustrated by the uncontrolled proliferation of cells with poor clinical prognosis [1]. There are various ways to control the cell proliferation. The new era of research is paying attention towards the development of anti-cancer agents that blocks the mitotic spindle during cell division [2]. These mitotic spindles are the rays which arise from microtubules and these microtubules are formed by polymerization of α - and β - tubulin heterodimer [3]. Compounds like colchicines, paclitaxel, vincristine are well known for tubulin inhibitors which interacts at different sites of β -tubulin and inhibit cell division by interfering with microtubule dynamics [4]. Due to the escalating multidrug resistance (MDR) of human cancer cells to the drugs *i.e.* paclitaxel and vincristine which interacts at

taxol and Vinca binding sites of tubulin respectively (due to the over expression of efflux pumps on cancer cells) [5,6], colchicine binding site inhibitors (CBSIs) have attracted great attention in search of new chemical entities that interact differently with tubulin [7]. Several natural as well as synthetic compounds with *cis* restricted geometries were developed which interact the tubulin at colchicine binding site [8]. Among the scaffolds, indole moiety has found to be versatile and several indole containing compounds were developed with excellent anti-proliferative activity [9]. Several indole based alkaloids have been explored to develop new anti-cancer agents from the natural as well as synthetic sources.

Topsentin is a *bis*-indole alkaloids found in several *Mediterranean shallow-water Sponges* such as *Topsentia genitrix*, *Spongosporites ruetzleri*, *Spongosorites genitrix* and *sponge Hexadella sp* [10]. It has received major

* Corresponding authors.

E-mail addresses: syedshafi@jamiyahamdard.ac.in (S. Shafi), yarmsy@rediffmail.com (M. Shahar Yar).

<https://doi.org/10.1016/j.bioorg.2019.103519>

Received 19 September 2019; Received in revised form 1 November 2019; Accepted 12 December 2019

Available online 23 December 2019

0045-2068/ © 2019 Elsevier Inc. All rights reserved.

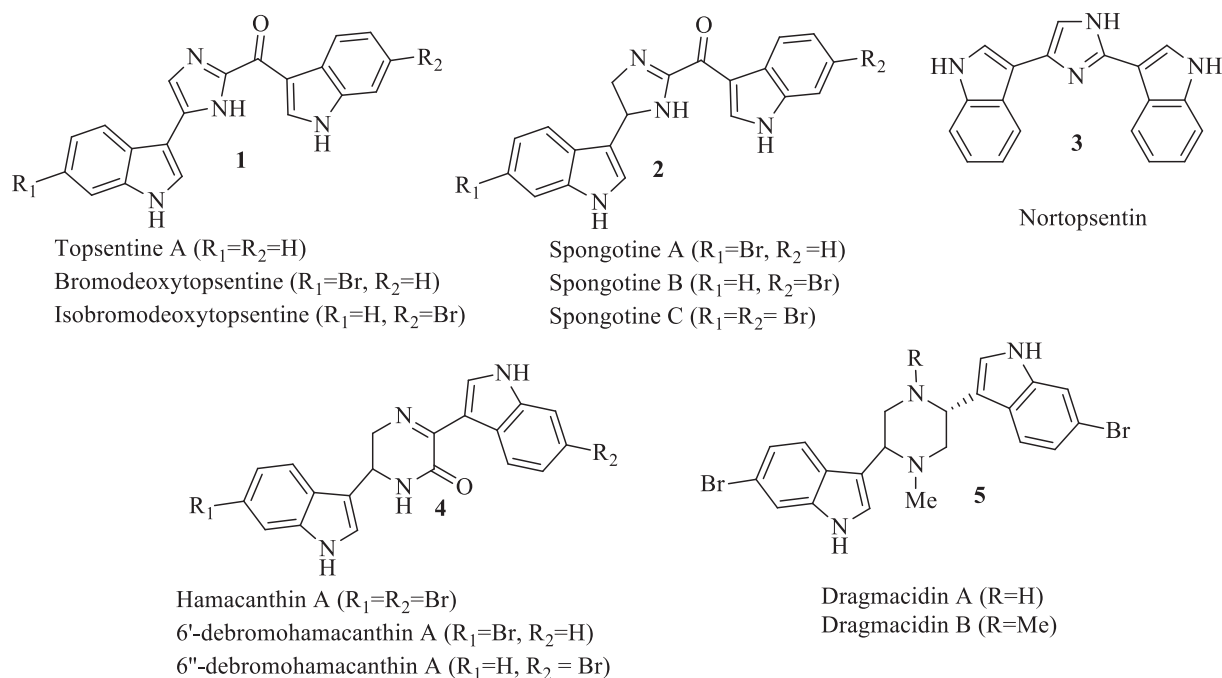


Fig. 1. Topsentine and other secondary metabolite of marine origin.

interest because of its broad spectrum of biological activities including anti-viral [11], anti-inflammatory [12], Anti-Alzheimers [10], and anti-proliferative [13] (IC_{50} between 6 and 20 $\mu g/mL$) activities [11]. Various other *bis*-indole containing secondary metabolites (1–5) [14] have also isolated from the marine invertebrate which have similar structural framework as that of topsentine as shown in Fig. 1.

Inspired by reported anti-proliferative activity of topsentine and its similarities with the structural template designed to develop the molecules that occupies the colchicines binding site, we aimed at the synthesis of 1,3,4-oxadiazole and 1,2,4-triazole based topsentine analogues that occupies colchicines binding site as demonstrated in Fig. 2.

2. Materials and methods

2.1. General

All the chemicals and reagents used in the study were purchased from Merck (India), Spectrochem, and Sigma Aldrich which were of reagent grade. TLC was performed for indication of reaction completion on 0.25 mm silica gel 60-F254 plates. UV light was used to visualize spots. Melting points of all the synthesized compounds were measured using Buchi labortechnik AG 9230 automated melting point apparatus (Switzerland); IR spectra were recorded on Bruker ALPHA FT-IR

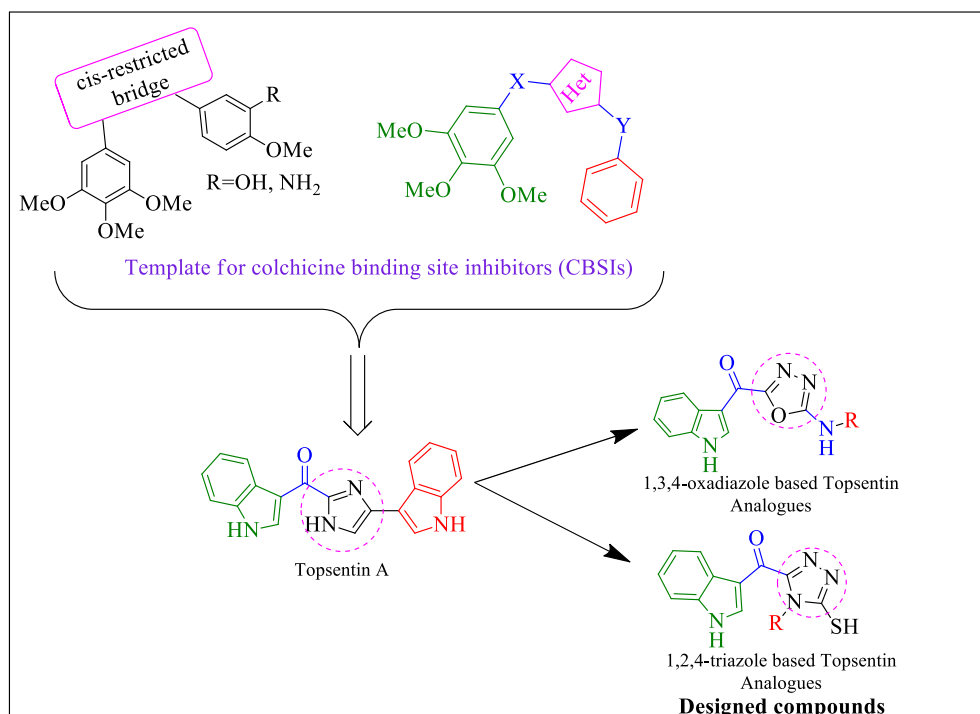


Fig. 2. Design strategy of 1,3,4-oxadiazole (11a-n) and 1,2,4-triazole (12a, c, e, g, h, j-n) based Topsentine analogues.

spectrometer (Germany), ^1H and ^{13}C NMR spectra were determined on a Bruker (300 MHz and 75 MHz) spectrometer and chemical shifts were expressed as ppm against TMS as internal reference. Mass spectras were recorded on ESI-MS. All compounds prepared in this paper are novel and confirmed with spectral data. All the synthesized compounds were recrystallized in methanol and were purified by column chromatography.

2.2. Chemistry

2.2.1. Procedure for synthesis of 2-(1H-indol-3-yl)-2-oxoacetyl chloride (7)

10 g of indole (6) was dissolved in 100 mL of diethyl ether. After complete dissolution, 10 mL of oxylyl chloride was added slowly to reaction mixture and stirred for 15 min. Orange colour precipitate 2-(1H-indol-3-yl)-2-oxoacetyl chloride (7) occurred in the reaction was filtered off and dried under high vacuum pump and immediately pursued for the further reaction without any delay.

2.2.2. Procedure for synthesis of 2-(1H-indol-3-yl)-2-oxoacetohydrazide (8)

Immediately, dried precipitate of compound 7 (10 g) was transferred slowly into a round bottomed flask with 100 mL of hydrazine hydrate for 15 min while stirring at ambient temperature. The reaction mixture was further allowed to stir at ambient temperature for further 30 min. After the completion of the reaction monitored by TLC (1:1 ratio of Ethyl acetate: Hexane), the reaction mixture was poured onto crushed ice. Creamish off white precipitates thus formed was filtered off and dried under vacuum. Creamish off white solid; 98% yield; ^1H NMR (400 MHz, DMSO- d_6) δ (ppm): 12.23 (s, 1H), 10.01 (s, 1H), 8.70 (s, 1H), 8.22–8.20 (m, 1H), 7.55–7.52 (m, 1H), 7.29–7.23 (m, 2H), 4.58 (s, 2H); MS (ESI) m/z : $[\text{M} + 1]^+$ 204.1.

2.2.3. General procedure for the synthesis of 2-(2-(1H-indol-3-yl)-2-oxoacetyl)-N-phenylhydrazine carbothioamide (10a-n)

0.5 g of compound 8 2-(1H-indol-3-yl)-2-oxoacetohydrazide and 0.53 g (1.2 equivalents) of different substituted aryl and alkyl isothiocyanates (9a-n) were refluxed in absolute ethanol (5 mL) for 6 hr. Solid precipitate was formed in the reaction mixture was filtered off and washed with cold alcohol to yield compounds (10a-n). TLC was run in TEF 4:5:1 which indicate the completion of the reaction.

2.2.4. Typical procedure for synthesis of 2-(2-(1H-indol-3-yl)-2-oxoacetyl)-N-phenylhydrazinecarbothioamide (10a)

To 10 mL of absolute ethanol, 2 g of compound 8 and 2.16 g (1.2 equivalents) of 1-isothiocyanato-4-nitrobenzene 9a was added and refluxed for 6 hr. after completion of reaction; solid precipitate was formed in reaction mixture. These Solid precipitate was filtered off and dried to afford compound 10a. Yellow solid; 86% yield; ^1H NMR (400 MHz, DMSO- d_6) δ (ppm): 12.29 (s, 1H), 10.85 (s, 1H), 10.19–10.13 (m, 2H), 8.79 (d, $J = 2.8$ Hz, 1H), 8.21–8.21 (m, 3H), 7.91 (d, $J = 8.8$ Hz, 2H), 7.57–7.55 (s, 1H), 7.30–7.27 (m, 2H); MS (ESI) m/z : $[\text{M} - 1]^+$ 382.3.

2.2.5. General procedure for the synthesis of (1H-indol-3-yl)(5-(phenylamino)-1,3,4-oxadiazol-2-yl)methanone (11a-n)

0.5 g of 2-(2-(1H-indol-3-yl)-2-oxoacetyl)-N-phenylhydrazinecarbothioamide (10a-n) and 0.832 g (3 equivalents) of N-(3-Dimethylaminopropyl)-N'-ethylcarbodiimide hydrochloride (EDC.HCl) with catalytic amount of Hydroxybenzotriazole (HOBt) were added to 5 mL of dry dimethylformamide (DMF). The reaction mixture was stirred for 3–5 h at room temperature under inert atmosphere. After the completion of reaction monitored by TLC (TEF, 4:5:1), the reaction mixture was poured onto ice. The precipitate formed was filtered off, washed with excess of water, dried under high vacuum and recrystallized in ethanol to afford the title compound 11a-n in pure form.

2.2.5.1. (1H-indol-3-yl)(5-((4-nitrophenyl)amino)-1,3,4-oxadiazol-2-yl)methanone (11a). Orange solid; 96% yield; mp 299.7 °C; IR (cm^{-1}): 3449, 3363, 3202, 3119, 3057, 2988, 2935, 1644, 1593, 1596, 1551, 1390, 1325, 1224, 1156, 1087, 843, 792, 735, 665, 609, 530; ^1H NMR (300 MHz, DMSO- d_6) δ (ppm): 12.40 (s, 1H), 11.81 (s, 1H), 8.89 (s, 1H), 8.32 (d, 3H, $J = 9.3$ Hz), 7.84 (d, 2H, $J = 9$ Hz), 7.58 (d, 1H, $J = 6.9$ Hz), 7.30 (t, 2H, $J = 3$ Hz); ^{13}C NMR (75 MHz, DMSO- d_6): 170.7, 160.3, 157.1, 154.9, 151.9, 138, 137, 126.4, 125.9, 124.1, 123.2, 121.7, 117.6, 113.8, 113.1; MS (ESI) m/z : $[\text{M} + 1]^+$ 350.1.

2.2.5.2. (1H-indol-3-yl)(5-((2-methoxyphenyl)amino)-1,3,4-oxadiazol-2-yl)methanone (11b). Yellow solid; 94% yield; mp 253 °C; 3456, 3211, 3040, 2965, 2892, 2847, 1637, 1610, 1589, 1545, 1505, 1554, 1222, 1153, 1126, 1069, 1030, 884, 855, 729, 630, 568, 520; ^1H NMR (300 MHz, DMSO- d_6) δ (ppm): 12.37 (s, 1H), 10.18 (s, 1H), 8.89 (s, 1H), 8.30 (d, 1H, $J = 4.80$ Hz), 8.01 (d, 1H, $J = 7.5$ Hz), 7.58 (d, 1H, $J = 5.1$ Hz), 7.30 (d, 2H, $J = 3.3$ Hz), 7.11 (s, 2H), 7.03 (d, 1H, $J = 6.0$ Hz), 3.89 (d, 3H, $J = 11.4$); ^{13}C NMR (75 MHz, DMSO- d_6): 170.9, 161.8, 157, 159.9, 137.9, 136.9, 127.3, 126.5, 124.6, 124, 123.1, 121.7, 121, 120.4, 113.8, 113.1, 112, 56.3; MS (ESI) m/z : $[\text{M} + 1]^+$ 335.2.

2.2.5.3. (1H-indol-3-yl)(5-((4-methoxyphenyl)amino)-1,3,4-oxadiazol-2-yl)methanone (11c). Yellow solid; 97% yield; mp 315.9 °C; 3432, 3347, 3188, 3055, 2994, 2937, 2899, 2811, 2757, 1650, 1599, 1509, 1554, 1223, 1159, 1081, 1041, 857, 827, 799, 772, 736, 602, 572, 530; ^1H NMR (300 MHz, DMSO- d_6) δ (ppm): 12.35 (s, 1H), 10.82 (s, 1H), 8.87 (s, 1H), 8.29–8.27(m, 1H), 7.59–7.53 (m, 3H), 7.32–7.27(m, 2H), 7.00–6.97 (m, 2H), 3.75 (s, 3H); ^{13}C NMR (75 MHz, DMSO- d_6): 170.9, 161.3, 156.7, 155.3, 137.8, 136.9, 131.8, 126.4, 124, 123.1, 121.7, 119.5, 115.8, 113.7, 113.1, 55.7; MS (ESI) m/z : $[\text{M} + 1]^+$ 335.1.

2.2.5.4. (5-((2-Fluorophenyl)amino)-1,3,4-oxadiazol-2-yl)(1H-indol-3-yl)methanone (11d). Yellow solid; 95% yield; mp 282 °C; IR (cm^{-1}): 3506, 3428, 3188, 3053, 2992, 2938, 2899, 2816, 1649, 1598, 1508, 1554, 1395, 1228, 1159, 1080, 1040, 857, 798, 736, 605, 566, 535; ^1H NMR (300 MHz, DMSO- d_6) δ (ppm): 12.38 (s, 1H), 10.85 (s, 1H), 8.85 (s, 1H), 8.31–8.28 (m, 1H), 8.11 (t, 1H, $J = 9$ Hz), 7.60–7.57 (m, 1H), 7.35–7.25 (m, 4H), 7.18 (t, 1H, $J = 6$ Hz); ^{13}C NMR (75 MHz, DMSO- d_6): 170.8, 161.4, 157.2, 154.8, 151.6, 137.9, 136.9, 126.4, 126.3, 125.2, 125, 124.9, 124.1, 123.1, 121.9, 121.7, 116.3, 116, 113.8, 113.1; MS (ESI) m/z : $[\text{M} + 1]^+$ 323.1.

2.2.5.5. (5-((4-Fluorophenyl)amino)-1,3,4-oxadiazol-2-yl)(1H-indol-3-yl)methanone (11e). Yellow solid; 94% yield; mp 332.7 °C; IR (cm^{-1}): 3506, 3428, 3188, 3053, 2992, 2938, 2899, 2816, 1649, 1598, 1508, 1555, 1395, 1290, 1228, 1159, 1080, 1040, 857, 798, 736, 605, 565, 535; ^1H NMR (300 MHz, DMSO- d_6) δ (ppm): 12.37 (s, 1H), 11.09 (s, 1H), 8.88 (s, 1H), 8.31–8.28 (m, 1H), 7.68–7.64 (m, 2H), 7.60–7.57 (m, 1H), 7.31–7.23 (m, 4H); ^{13}C NMR (75 MHz, DMSO- d_6): 170.9, 161, 159.7, 156.7, 137.9, 136.9, 135, 126.4, 124.1, 123.1, 121.7, 119.5, 119.4, 116.4, 116.1, 113.7, 113.1; MS (ESI) m/z : $[\text{M} + 1]^+$ 323.1.

2.2.5.6. (5-((3-Chlorophenyl)amino)-1,3,4-oxadiazol-2-yl)(1H-indol-3-yl)methanone (11f). Yellow solid; 97% yield; mp 321.3 °C; IR (cm^{-1}): 3448, 3361, 3202, 3118, 3058, 2988, 2937, 1643, 1594, 1595, 1551, 1224, 1156, 1088, 1012, 887, 850, 792, 735, 664, 609, 529; ^1H NMR (300 MHz, DMSO- d_6) δ (ppm): 12.38 (s, 1H), 11.29 (s, 1H), 8.88 (s, 1H), 8.31–8.28 (m, 1H), 7.81 (s, 1H), 7.60–7.52 (m, 2H), 7.45–7.39 (m, 1H), 7.31–7.26 (m, 2H), 7.12 (d, 1H, $J = 7.2$ Hz); ^{13}C NMR (75 MHz, DMSO- d_6): 170.8, 164.2, 160.6, 156.8, 150.1, 138, 136.9, 134, 131.3, 126.4, 124.1, 123.1, 122.5, 121.7, 117.2, 116.4, 113.7, 113.1; MS (ESI) m/z : $[\text{M} + 1]^+$ 339.

2.2.5.7. (5-((4-Chlorophenyl)amino)-1,3,4-oxadiazol-2-yl)(1H-indol-3-yl)methanone (11g). Yellow solid; 98% yield; mp 334.4 °C; IR (cm^{-1}):

3445, 3358, 3325, 3286, 3209, 3118, 3058, 3028, 2991, 2940, 1644, 1597, 1593, 1552, 1390, 1222, 1157, 1092, 1012, 854, 829, 794, 736, 667, 605, 527; ¹H NMR (300 MHz, DMSO-*d*₆) δ (ppm): 12.40 (s, 1H), 11.24 (s, 1H), 8.88 (s, 1H), 8.30 (d, 1H, *J* = 4.5 Hz), 7.70–7.65 (m, 2H), 7.60–7.57 (s, 1H), 7.49–7.45 (m, 2H), 7.31–7.28 (m, 2H); ¹³C NMR (75 MHz, DMSO-*d*₆): 170.9, 160.8, 156.8, 137.9, 137.6, 136.9, 129.5, 126.5, 126.4, 124.1, 123.1, 121.7, 119.4, 113.7, 113.1 MS (ESI) *m/z*: [M+1]⁺ 339.1.

2.2.5.8. (5-((3-Bromophenyl)amino)-1,3,4-oxadiazol-2-yl)(1H-indol-3-yl)methanone (11h). Yellow solid; 92% yield; mp 277.3 °C; IR (cm⁻¹): 3446, 3358, 3326, 3286, 3209, 3118, 3058, 3028, 2990, 2940, 1643, 1596, 1541, 1593, 1552, 1390, 1222, 1157, 1091, 854, 829, 793, 736, 661, 607, 528; ¹H NMR (300 MHz, DMSO-*d*₆) δ (ppm): 12.39 (s, 1H), 11.29 (s, 1H), 8.89 (s, 1H), 8.31–8.28 (m, 1H), 7.96 (s, 1H), 7.58 (d, 2H, *J* = 6 Hz), 7.39–7.20 (m, 4H); ¹³C NMR (75 MHz, DMSO-*d*₆): 170.8, 162.1, 157.3, 137.9, 136.6, 133.6, 129, 127.2, 126.4, 123.1, 121.7, 117, 113.7, 113.1; MS (ESI) *m/z*: [M]⁺ 382, [M+1]⁺ 383, [M+2]⁺ 384.

2.2.5.9. (5-((2-Bromophenyl)amino)-1,3,4-oxadiazol-2-yl)(1H-indol-3-yl)methanone (11i). Yellow solid; 94% yield; mp 256.4 °C; IR (cm⁻¹): 3447, 3359, 3206, 3118, 3058, 2989, 2939, 1643, 1595, 1594, 1551, 1390, 1223, 1156, 1090, 853, 831, 793, 736, 663, 609, 528; ¹H NMR (300 MHz, DMSO-*d*₆) δ (ppm): 12.35 (s, 1H), 10.38 (s, 1H), 8.86 (s, 1H), 8.29–8.26 (m, 1H), 7.89 (d, 1H, *J* = 8.1 Hz), 7.73 (d, 1H, *J* = 7.8 Hz), 7.59–7.56 (m, 1H), 7.47 (t, 1H, *J* = 7.5), 7.32–7.25 (m, 2H), 7.18 (t, 1H, *J* = 7.5 Hz); ¹³C NMR (75 MHz, DMSO-*d*₆): 170.8, 162.1, 157.3, 137.9, 136.9, 136.6, 133.6, 129, 127.2, 126.4, 125.2, 124.1, 123.1, 121.7, 117, 113.7, 113.1; MS (ESI) *m/z*: [M]⁺ 382, [M+1]⁺ 383, [M+2]⁺ 384.

2.2.5.10. (5-((4-Ethoxyphenyl)amino)-1,3,4-oxadiazol-2-yl)(1H-indol-3-yl)methanone (11j). Yellow solid; 96% yield; mp 358.7 °C; 3505, 3427, 3188, 3053, 2992, 2939, 2816, 1650, 1598, 1508, 1555, 1395, 1229, 1159, 1080, 1040, 798, 736, 605; ¹H NMR (300 MHz, DMSO-*d*₆) δ (ppm): 12.36 (s, 1H), 10.83 (s, 1H), 8.88 (s, 1H), 8.31–8.28 (m, 1H), 7.59–7.53 (m, 3H), 7.38–7.26 (m, 2H), 6.97 (d, 2H, *J* = 9 Hz); 4.00 (q, 2H, *J* = 6.6 Hz), 1.32 (t, 3H, *J* = 6.9); ¹³C NMR (75 MHz, DMSO-*d*₆): 170.9, 161.3, 156.6, 154.6, 137.8, 136.9, 131.6, 126.4, 124, 123.1, 121.7, 119.4, 115.4, 113.7, 113.1, 63.6, 15.1; MS (ESI) *m/z*: [M+1]⁺ 349.1.

2.2.5.11. (5-(Benzylamino)-1,3,4-oxadiazol-2-yl)(1H-indol-3-yl)methanone (11k). Creamish white solid; 95% yield; mp 301.6 °C; IR (cm⁻¹): 3448, 3360, 3203, 3118, 3058, 2988, 2937, 1643, 1594, 1595, 1551, 1390, 1223, 1156, 1089, 1012, 977, 887, 851, 792, 735, 664, 609, 529; ¹H NMR (300 MHz, DMSO-*d*₆) δ (ppm): 12.29 (s, 1H), 8.81 (d, 2H, *J* = 4.2 Hz), 8.27 (d, 1H, *J* = 6 Hz), 7.55 (d, 1H, *J* = 7.5 Hz), 7.39–7.34 (m, 4H), 7.31–7.26 (m, 3H), 4.52 (d, 2H, *J* = 5.7 Hz); ¹³C NMR (75 MHz, DMSO-*d*₆): 171, 164.6, 157.2, 138.7, 137.5, 136.9, 128.9, 127.8, 127.7, 126.4, 123.9, 123, 121.7, 113.6, 113, 46.4; MS (ESI) *m/z*: [M+1]⁺ 319.1.

2.2.5.12. (5-(Butylamino)-1,3,4-oxadiazol-2-yl)(1H-indol-3-yl)methanone (11l). Creamish white solid; 89% yield; mp 256 °C; IR (cm⁻¹): 3517, 3448, 3362, 3202, 3118, 3058, 2988, 2936, 1644, 1594, 1596, 1551, 1390, 1224, 1156, 1088, 846, 792, 735, 664, 609, 530; ¹H NMR (300 MHz, DMSO-*d*₆) δ (ppm): 12.28 (s, 1H), 8.82 (s, 1H), 8.29–8.23 (m, 2H), 7.58–7.55 (m, 1H), 7.31–7.24 (m, 2H), 3.30 (q, 2H, *J* = 6.6 Hz), 1.63–1.53 (m, 2H), 1.43–1.31 (m, 2H), 0.92 (t, 3H, *J* = 7.2 Hz); ¹³C NMR (75 MHz, DMSO-*d*₆): 171.1, 164.6, 157, 137.4, 136.9, 126.5, 123.9, 122.9, 121.7, 113.6, 113, 42.6, 31.2, 19.8, 15; MS (ESI) *m/z*: [M+1]⁺ 285.1.

2.2.5.13. (5-(Cyclohexylamino)-1,3,4-oxadiazol-2-yl)(1H-indol-3-yl)

methanone (11m). Creamish white solid; 97% yield; mp 306.3 °C; IR (cm⁻¹): 3448, 3362, 3202, 3119, 3057, 2988, 2935, 1644, 1593, 1596, 1551, 1224, 1156, 1087, 843, 792, 735, 665, 609, 530; ¹H NMR (300 MHz, DMSO-*d*₆) δ (ppm): 12.28 (s, 1H), 8.81 (s, 1H), 8.26 (t, 2H, *J* = 7.8 Hz), 7.57–7.54 (m, 1H), 7.30–7.23 (m, 2H), 1.97 (s, 2H), 1.73 (s, 2H), 1.58 (d, 1H, *J* = 10.8 Hz), 1.36–1.26 (m, 5H); ¹³C NMR (75 MHz, DMSO-*d*₆): 171.1, 163.9, 156.9, 137.4, 136.9, 126.5, 123.9, 122.9, 121.7, 113.6, 113, 52.3, 32.6, 25.5, 24.7; MS (ESI) *m/z*: [M+1]⁺ 311.1.

2.2.5.14. (5-(Ethylamino)-1,3,4-oxadiazol-2-yl)(1H-indol-3-yl)methanone (11n). Creamish white solid; 80% yield; mp 232.9 °C; IR (cm⁻¹): 3496, 3440, 3348, 3268, 3223, 3161, 3117, 3016, 2982, 2936, 2887, 2859, 2813, 1607, 1598, 1546, 1229, 1127, 1053, 854, 795, 769, 737, 693, 647, 594, 542, 530; ¹H NMR (300 MHz, DMSO-*d*₆) δ (ppm): 12.29 (s, 1H), 8.81 (s, 1H), 8.26 (d, 2H, *J* = 7.5 Hz), 7.56 (d, 1H, *J* = 8.1 Hz), 7.27 (t, 2H, *J* = 3.6), 3.91–3.83 (m, 2H), 1.23–1.18 (m, 3H); ¹³C NMR (75 MHz, DMSO-*d*₆): 171.1, 164.4, 157, 137.4, 136.8, 126.4, 123.9, 123, 121.7, 113.6, 113, 37.9, 15.9; MS (ESI) *m/z*: [M+1]⁺ 255.4.

2.2.6. General procedure for the synthesis of (1H-indol-3-yl)(5-mercapto-4-phenyl-4H-1,2,4-triazol-3-yl)methanone (12a, c, e, g, h, j-n)

To the methanolic solution of 2-(2-(1H-indol-3-yl)-2-oxoacetyl)-*N*-phenylhydrazinecarbothioamide (0.1 g) (**10a-n**) 2 N solution of NaOH (10 mL) was added to it and refluxed for 12 h. After completion, reaction was monitored by TLC (run in TEF 4:5:1), reaction mixture was poured onto crushed ice and was acidified with 2 N HCl to give the solid precipitate. The solid precipitate was filtered off, washed with excess of water, dried under high vacuum and recrystallized in ethanol to yield pure compounds (**12a, c, e, g, h, j-n**).

2.2.6.1. (1H-indol-3-yl)(5-mercapto-4-(4-nitrophenyl)-4H-1,2,4-triazol-3-yl)methanone (12a). Orange solid; 96% yield; mp 290.5 °C; IR (cm⁻¹): 3439, 3398, 3289, 3228, 3107, 2575, 1709, 1591, 1509, 1448, 1342, 1087, 850, 792, 742, 676, 614; ¹H NMR (300 MHz, DMSO-*d*₆) δ (ppm): 12.42 (s, 1H), 11.87 (s, 1H), 8.90 (d, 1H, *J* = 2.1 Hz), 8.32 (d, 3H, *J* = 8.7 Hz), 7.84 (d, 2H, *J* = 8.7 Hz), 7.58 (d, 1H, *J* = 5.7 Hz), 7.31–7.29 (m, 2H); ¹³C NMR (75 MHz, DMSO-*d*₆): 170.7, 160.2, 157.1, 144.7, 142, 138.1, 136.9, 126.3, 125.9, 124.1, 123.2, 121.7, 117.6, 113.7, 1133.2; MS (ESI) *m/z*: [M]⁺ 365.

2.2.6.2. (1H-indol-3-yl)(5-mercapto-4-(4-methoxyphenyl)-4H-1,2,4-triazol-3-yl)methanone (12c). Yellow solid; 87% yield; mp 253.9 °C; IR (cm⁻¹): 3484, 3336, 3275, 3120, 3043, 2911, 2535, 1639, 1597, 1509, 1433, 1300, 1235, 1141, 1009, 750, 609, 570; ¹H NMR (300 MHz, DMSO-*d*₆) δ (ppm): 14.33 (s, 1H), 12.36 (s, 1H), 10.83 (s, 1H), 8.88 (d, 1H, *J* = 3.3 Hz), 8.53 (d, 1H, *J* = 3 Hz), 8.04 (d, 1H, *J* = 7.5 Hz), 7.56–7.52 (m, 2H), 7.37–7.13 (m, 3H), 7.02 (d, 2H, *J* = 8.7 Hz), 3.80 (s, 3H); ¹³C NMR (75 MHz, DMSO-*d*₆): 169.8, 159.7, 139.2, 137.8, 137.1, 136.9, 129.4, 127.7, 126, 124.1, 123.1, 121.7, 121.5, 119.4, 114.8, 114.4, 113, 55.8; MS (ESI) *m/z*: [M+1]⁺ 351.2.

2.2.6.3. (4-(4-Fluorophenyl)-5-mercapto-4H-1,2,4-triazol-3-yl)(1H-indol-3-yl)methanone (12d). Yellow solid; 87% yield; mp 278.3 °C; IR (cm⁻¹): 3387, 3356, 3217, 3049, 2922, 2581, 1611, 1578, 1502, 1447, 1388, 1223, 1201, 1136, 1057, 881, 851, 779, 730, 658, 628, 572; ¹H NMR (300 MHz, DMSO-*d*₆) δ (ppm): 14.41 (s, 1H), 12.38 (s, 1H), 11.11 (s, 1H), 8.88 (s, 1H), 8.56 (s, 1H), 8.03 (d, 1H, *J* = 7.8 Hz), 7.67–7.63 (m, 1H), 7.58–7.52 (m, 1H), 7.47–7.43 (m, 1H), 7.36–7.17 (m, 3H); MS (ESI) *m/z*: [M-2]⁺ 336.3.

2.2.6.4. (4-(4-Chlorophenyl)-5-mercapto-4H-1,2,4-triazol-3-yl)(1H-indol-3-yl)methanone (12g). Yellow solid; 65% yield; mp 291.5 °C; IR (cm⁻¹): 3444, 3230, 3102, 3046, 2586, 1633, 1598, 1482, 1419, 1304, 1237, 1090, 1003, 938, 856, 750, 676, 606, 540; ¹H NMR

(300 MHz, DMSO- d_6) δ (ppm): 14.38 (s, 1H), 12.37 (s, 1H), 11.22 (s, 1H), 8.88 (s, 1H), 8.04 (d, 1H, $J = 7.5$ Hz), 7.68–7.53 (m, 3H), 7.47–7.38 (m, 2H), 7.29–7.18 (m, 2H); ^{13}C NMR (75 MHz, DMSO- d_6): 174, 169.7, 148.3, 139.1, 137, 134.3, 134, 130.2, 129.4, 126.1, 124.2, 123.2, 121.5, 119.4, 114.6, 112.7; MS (ESI) m/z : $[\text{M} - 1]^+$ 353.2.

2.2.6.5. (4-(3-Bromophenyl)-5-mercapto-4H-1,2,4-triazol-3-yl)(1H-indol-3-yl)methanone (**12h**). Yellow solid; 65% yield; mp 193.8 °C; IR (cm^{-1}): 3460, 3416, 3264, 3144, 3003, 2914, 2845, 2555, 1701, 1598, 1542, 1505, 1438, 1284, 1210, 1115, 1066, 1015, 878, 844, 735, 622; ^1H NMR (300 MHz, DMSO- d_6) δ (ppm): 14.49 (s, 1H), 12.40 (s, 1H), 11.31 (s, 1H), 8.89 (d, 1H, $J = 3$ Hz), 8.57 (d, 1H, $J = 3.3$ Hz), 7.96 (s, 1H), 7.58–7.50 (m, 2H), 7.48–7.20 (m, 4H); ^{13}C NMR (75 MHz, DMSO- d_6): 177.1, 174, 163.3, 139.3, 136.7, 130.9, 130.3, 128.7, 127.6, 125.9, 125.4, 122.6, 123.4, 120.9, 112; MS (ESI) m/z : $[\text{M} - 1]^+$ 400.2.

2.2.6.6. (4-(4-Ethoxyphenyl)-5-mercapto-4H-1,2,4-triazol-3-yl)(1H-indol-3-yl)methanone (**12j**). Orange solid; 60% yield; mp 262 °C; IR (cm^{-1}): 3455, 3304, 3231, 3099, 3041, 2973, 2594, 1639, 1604, 1514, 1480, 1432, 1304, 1268, 1229, 1146, 1119, 1033, 857, 825, 747, 647; ^1H NMR (300 MHz, DMSO- d_6) δ (ppm): 14.32 (s, 1H), 12.37 (s, 1H), 10.83 (s, 1H), 8.88 (d, 1H, $J = 2.1$ Hz), 8.54 (d, 1H, $J = 2.4$ Hz), 8.04 (d, 1H, $J = 7.8$ Hz), 7.54 (d, 1H, $J = 8.1$ Hz), 7.29–7.18 (m, 3H), 7.00 (d, 2H, $J = 7.8$ Hz), 4.06 (q, 2H, $J = 6.9$ Hz), 1.35 (t, 2H, $J = 6.9$ Hz); ^{13}C NMR (75 MHz, DMSO- d_6): 174.4, 169.8, 159.0, 148.8, 139.2, 137.1, 129.4, 127.5, 126.0, 124.1, 123.1, 121.5, 115.4, 114.9, 114.8, 113.1, 63.7, 15.11; MS (ESI) m/z : $[\text{M} + 1]^+$ 365.2.

2.2.6.7. (4-Benzyl-5-mercapto-4H-1,2,4-triazol-3-yl)(1H-indol-3-yl)methanone (**12k**). Creamish white solid; 98% yield; mp 258.8 °C; IR (cm^{-1}): 3474, 3396, 3289, 3121, 3093, 2975, 2925, 2643, 1673, 1633, 1524, 1478, 1436, 1417, 1360, 1268, 1120, 1011, 884, 855, 774, 727, 629, 551; ^1H NMR (300 MHz, DMSO- d_6) δ (ppm): 14.53 (s, 1H), 12.34 (s, 1H), 8.54 (s, 1H), 7.55 (d, 1H, $J = 1.5$ Hz), 7.38–7.21 (m, 7H), 5.62 (s, 2H); ^{13}C NMR (75 MHz, DMSO- d_6): 174.9, 169.3, 147.5, 138.6, 136.9, 128.8, 127.7, 127.5, 126.3, 124.1, 123.2, 121.7, 114.2, 113.1, 47.4; MS (ESI) m/z : $[\text{M} + 1]^+$ 335.2.

2.2.6.8. (4-Butyl-5-mercapto-4H-1,2,4-triazol-3-yl)(1H-indol-3-yl)methanone (**12i**). Pale Yellow solid; 70% yield; mp 225.9 °C; IR (cm^{-1}): 3367, 3100, 3043, 2960, 2925, 2560, 1613, 1581, 1512, 1474, 1418, 1361, 1270, 1196, 1118, 998, 884, 854, 746, 643, 560, 529; ^1H NMR (300 MHz, DMSO- d_6) δ (ppm): 14.29 (s, 1H), 12.35 (s, 1H), 10.83 (s, 1H), 8.52 (s, 1H), 8.27 (d, 1H, $J = 5.1$ Hz), 7.56 (d, 1H, $J = 7.2$ Hz), 7.29 (m, 2H), 4.32–4.27 (m, 2H), 1.71–1.66 (m, 2H), 1.34–1.27 (m, 2H), 0.88 (t, 2H, $J = 7.2$ Hz); ^{13}C NMR (75 MHz, DMSO- d_6): 175.3, 168.5, 147.8, 138.7, 137, 126.3, 124.18, 123.2, 121.77, 114.5, 113.1, 44.4, 30.7, 19.7, 14; MS (ESI) m/z : $[\text{M} + 1]^+$ 301.2.

2.2.6.9. (4-Cyclohexyl-5-mercapto-4H-1,2,4-triazol-3-yl)(1H-indol-3-yl)methanone (**12m**). Creamish white solid; 92% yield; mp 251.3 °C; IR (cm^{-1}): 3443, 3334, 3206, 3161, 2927, 2569, 1713, 1626, 1518, 1430, 1341, 1204, 1149, 1119, 1021, 856, 744, 650, 606; ^1H NMR (400 MHz, DMSO- d_6) δ (ppm): 14.19 (s, 1H), 12.44 (s, 1H), 8.33 (s, 1H), 7.81 (s, 1H), 7.56–7.50 (m, 3H), 7.32–7.28 (m, 2H), 4.66 (t, $J = 11.6$ Hz, 1H), 2.24–2.15 (m, 2H), 1.84–1.52 (m, 4H), 1.32–1.08 (m, 4H); ^{13}C NMR (75 MHz, DMSO- d_6): 174.6, 162.7, 157, 136.7, 130.9, 125.4, 120.9, 112.0, 52.9, 25.9; MS (ESI) m/z : $[\text{M} - 1]^+$ 325.3.

2.2.6.10. (4-Ethyl-5-mercapto-4H-1,2,4-triazol-3-yl)(1H-indol-3-yl)methanone (**12n**). Pale yellow solid; 81% yield; mp 276.3 °C; IR (cm^{-1}): 3408, 3278, 3102, 3042, 2878, 2582, 1649, 1607, 1512, 1478, 1445, 1341, 1277, 1203, 1146, 1118, 1086, 987, 860, 792, 777, 743, 652, 604; ^1H NMR (300 MHz, DMSO- d_6) δ (ppm): 14.30 (s, 1H), 12.34 (s, 1H), 8.52 (s, 1H), 8.29–8.26 (m, 1H), 7.57–7.55 (m, 1H), 7.30–7.27 (m, 2H), 4.32 (q, 2H, $J = 6.6$ Hz), 1.30 (t, 3H, $J = 6.9$ Hz);

^{13}C NMR (75 MHz, DMSO- d_6): 175.2, 168.2, 147.8, 138.7, 136.9, 126.2, 124.0, 123.0, 121.7, 114.5, 113.0, 42.8, 14.2; MS (ESI) m/z : $[\text{M} - 1]^+$ 271.2.

2.3. Pharmacology

2.3.1. Sixty cancer cell line screening at the NCI

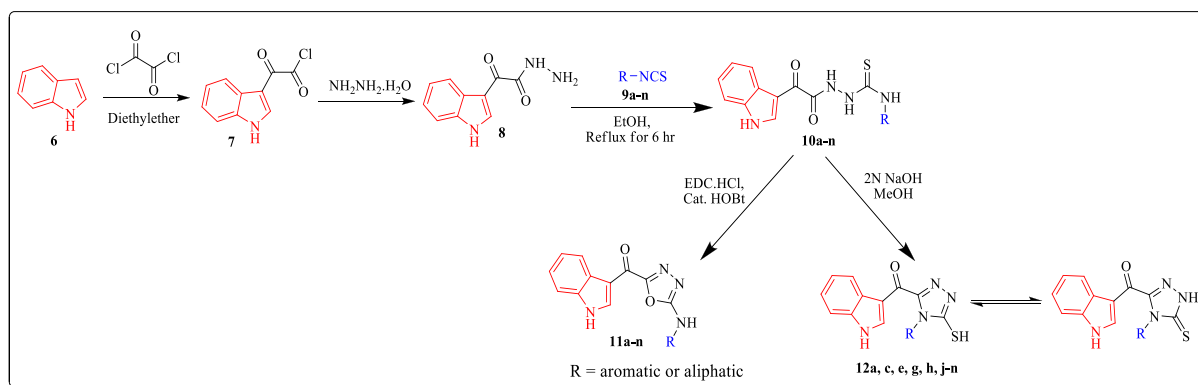
All the synthesized compounds were screened for their anti-proliferative activity against a panel of 60 cancer cell line at National Cancer Institute, Bethesda, MD, USA as per the standard procedure given at <http://www.dtp.nci.nih.gov> [15]. RPMI 1640 medium (5% fetal bovine serum and 2 mM L-glutamine) was used to grow the human tumor cell lines. All the tumor cells were incubated into 96-well microtiter plate. Then this plated was placed for incubation at 37 °C for 24 h. After that two plates of each cell line were fixed with TCA *in situ* and optical density was measured at this point which represented the cell population of each cell line at the time of compound addition (ODzero). On the other hand, all the tested compounds were dissolved in DMSO to yield 400-fold desired final concentration and stored at –80 °C. These frozen compounds were thawed and their aliquot part was diluted to 10^{-4} M concentration with the medium containing 50 $\mu\text{g}/\text{mL}$ of gentamicin at the time of compound addition. Control sample was made with DMSO only. 100 μl of the tested compounds from the aliquot parts were added to appropriate 96-well microtiter plate containing 100 μl of medium ensuing in the required final drug concentrations of 10^{-5} M and 0 M (control). After addition of tested compounds, 96-well microtiter plate was incubated for 48 h at 100%, 5% CO_2 , 95% air, 100% relative humidity. Cold TCA was used to stop the assay for adherent cells. Further on 50 mL of 50% (w/v) TCA was used to fix the cell and incubated for 1 hr at 4 °C. The supernatant was removed, and the 96-well microtiter plates were rinsed five times with water and air dried. 100 mL solution of protein binding dye, Sulforhodamine B (SRB) was made at 0.4% (w/v) in 1% acetic acid and was added to each well of the plates. These Plates were placed at room temperature for incubation for 10 min then were washed with 1% acetic acid five times to remove unbound dye. Then the plates were treated with 10 Mm trizma base, so that unbound dye was solubilized with trizma base. The absorbance was measured at a wavelength of 515 nm on an automated plate reader and results for each tested compounds were calculated as the percent of tumor growth of the treated cells in comparison with the untreated control cells. Optical density (OD) was recored for SRB-derived color just before exposing the cells to the test compound (ODzero) and after 48hrs exposure to the test compound (ODtest) or the control vehicle (ODctrl).

2.3.2. Anti-proliferative assay against MCF-7 cancer cell line

Compounds **11a**, **11d**, **11f**, **12e**, and **12h**, showed consistent activity against MCF-7 Breast cancer cell line with lower % growth and was selected to evaluate its anti-proliferative activity against MCF-7 cancer cell line using MTT assay [16]. Doxorubicin and combretastatin A-4 (CBSIs) were used as a standard. Cancer cells were seeded on 96-well plate ($3-5 \times 10^3$ cells per well) and incubated for 48 h at 37 °C then treated with different concentration of the test compound with respective to vehicle control. After 48 h of incubation, it was exposed to 20 μl of freshly prepared MTT reagent (3-(4, 5-dimethylthiazol-2-yl)-2,5-diphenyl tetrazolium bromide) incubated for 2 h. The supernatant from each well was removed and replaced with DMSO (100 μl) to dissolve formazan crystal. The optical density (absorbance) was recorded at 570 nm with reference wavelength of 620 nm and its half maximal inhibitory concentration (IC_{50}) was calculated from the equation of the dose response curve.

2.3.3. Cell cycle analysis

Effect of **11d** on the cell cycle of MCF-7 cell line was evaluated by using flow cytometry at 0.5 μM , 1 μM , 2 μM , 5 μM and 10 μM concentration. These cells were seeded into 6 well plates and placed for



Scheme 1. Protocol for the synthesis of indole linked 1,3,4-oxadiazole conjugates (**11a-n**) and 1,2,4-triazole conjugates (**12a, c, e, g, h, j-n**).

incubation at 37 °C for 24 h which lead to attachment of cells with 50–60% confluency. Further on it was treated with vehicle control 0.1% DMSO and **11d** (0.5, 1, 2, 5 and 10 μ M) and incubated for 72 h. The collected cells were harvested and fixed with 75% ice cold ethanol at 4 °C. Excess of ethanol was removed and cells were washed with PBS. Cells were treated and stained with RNase (50 U/mL) and Propidium Iodide (20 μ g/mL) staining solution for 20 min at room temperature in dark and was further subjected for flow cytometry (Bectone Dickinson, FACS Calibur system) [17].

2.3.4. Wound healing assay

To evaluate the effect of **11d** on cell migration, wound healing assay was performed [18]. Firstly, MCF-7 cells (3×10^5) were seeded and grown to each well of 6 well plates until mono-layer was formed. Then by using 200 μ l pipette tip, a scratches were made in confluent monolayers. After this, the wounds were washed with PBS to remove non-adherent cell debris. Cells were further treated with 5 μ M and 10 μ M of **11d**. Cells which migrated across the wound area were captured with an inverted microscope and photographed for indicated time (0, 8, 16 and 24 h).

2.3.5. Mitochondrial membrane potential analysis

JC-1 staining method was opted to study the effect of **11d** on mitochondrial membrane potential of MCF-7 cells [19]. Briefly, MCF-7 cells treated with **11d** at 5 μ M and 10 μ M for 72 h and were incubated with 10 μ M JC-1 dye diluted in PBS for 20 min at 37 °C, 5% CO₂ incubator. Monomer was treated with excited wavelength of 488 nm. A green fluorescence is emitted by JC-1 monomers with a maximum emission at 530 nm, where as J-aggregates emitted orange-red fluorescence maximum at 590 nm.

2.3.6. In vitro tubulin polymerization inhibitory assay

The compounds **11d** and **12e** were monitored for their anti-tubulin activity. Study involved *in vitro* assay to monitor the time dependent polymerization of tubulin into microtubules using fluorescence-based tubulin polymerization assay kit (BK011, Cytoskeleton, Inc.) as per manufacturer's protocol [20]. Experiment involved measurement of fluorescence emission at 420 nm (excitation wavelength at 360 nm) for 1 h in a multimode plate reader (Tecan M200 infinite). For the two test compounds (**11d** and **12e**), standard (Nocodazole) and control (zero drug), the reaction mixture was prepared separately as per specification of cytoskeleton protocol for tubulin inhibition. In brief, 2 mg/ml tubulin in 80 mM PIPES with pH 6.9, 2 nM MgCl₂, 0.5 mM EGTA, 1.0 mM GTP and 15% tubulin glycerol were taken in a final volume of 50 μ l and transferred into each well of 96 well microplate (Prior to transfer of reaction mixture the plate was warmed up to 37 °C for 10 min. For determination of IC₅₀ values of two compounds against tubulin polymerization, the compounds were pre-incubated with tubulin at varying concentrations (1, 5 and 10 μ M).

2.3.7. Molecular docking

To view binding pattern of all the synthesized compounds for anti-proliferative activity, molecular docking was done at colchicine binding site (chain B) of β -tubulin (PDB code: 1SA0) [21]. The docking simulations of all the compounds were performed using Maestro, version 9.6 implemented from Schrodinger software suite. Synthesized compounds were sketched in 3D format using the build panel and were also prepared for docking using lig prep application. The proteins were taken from Protein data bank and were prepared for docking by solvent removing, hydrogen adding and further minimization in the presence of bound ligand (COL) using protein preparation wizard. Grids for molecular docking were generated with bound co-crystallized ligand. For validation of docking parameters co-crystal ligand (COL) was re-docked at catalytic site of protein. RMSD between co-crystal and re-docked pose was found to be 0.235 Å [22]. Compounds were docked using Glide extra-precision (XP) mode, with up to three poses saved per molecule.

3. Result and discussion

3.1. Chemistry

Above designed Indole linked 1,3,4-oxadiazole conjugates (**11a-n**) and 1,2,4-triazole (**12a, c, e, g, h, j-n**) and were synthesized as outline in Scheme 1. Indole 6 was reacted with the oxalyl chloride to give 2-(1H-indol-3-yl)-2-oxoacetyl chloride 7 [23] which was then reacted with the hydrazine hydrate to form 2-(1H-indol-3-yl)-2-oxoacetohydrazide 8. Compound 8 was further refluxed with different aliphatic as well as aryl isothiocyanates (**9a-n**) to afford different substituted thiosemicarbazides (**10a-n**). These thiosemicarbazides (**10a-n**) were cyclized under coupling conditions with *N*-Ethyl-*N'*-(3-dimethylamino-propyl)carbodiimide hydrochloride (EDC.HCl) & Hydroxybenzotriazole (HOBT) to afford substituted 1,3,4-oxadiazoles (**11a-n**) in very good yields (90–95%). On the another side, thiosemicarbazides (**10a-n**) cyclized with 2 N NaOH to afford 5-mercapto-1,2,4-triazoles (**12a, c, e, g, h, j-n**) in 60–70% yields as illustrated in Table 1.

Formation of *N*-substituted 2-amino-1,3,4-oxadiazole (**11a-n**) from thiosemicarbazides (**10a-n**) was confirmed by the appearance of a singlet corresponds to –NH proton at in the range of δ 10.18–11.81 and disappearance of two NH peak at 10.85 and 10.13 corresponds to amides in ¹H NMR (supplementary data). The presence of two singlets in the range at δ 12.29–12.39 and δ 10.18–11.81 corresponds to indolyl –NH and –NH of 2-amino-1,3,4-oxadiazole (**11a-n**) respectively was evidenced by D₂O exchange ¹H NMR spectra of **11c** (supplementary data). While ¹³C NMR gave two characteristic peaks for these derivative i.e C=O at δ 171.11–170.75 ppm and –O–C(=N)–NH at δ 160.37–164.62 ppm. All the intermediates and target compounds were finally confirmed by their mass spectras.

Formation of thiosemicarbazide (**10a-n**) from hydrazide (**8**) was

confirmed by the appearance of four singlets corresponds to $-NH$ groups at δ 12.29, 10.85, 10.19, and 10.13 ppm in 1H NMR (10a). Base catalysed cyclization was confirmed by the appearance of a singlet corresponds to $-SH$ proton at δ 14.30–14.66 ppm and the disappearance of three singlets corresponding to $-NH$ groups of thiosemicarbazide. 5-mercapto-1,2,4-triazoles with aromatic substitution on nitrogen (12a, c, e, g, h, j) were observed as tautomers in different ratios as observed from 1H NMR (supplementary data). Appearance of a singlet corresponds to $-NH$ proton at δ 10.43–11.87 ppm confirmed the existence of its tautomer. It was further confirmed by IR which obtained absorption bands for $S-H$ at $2535-2643\text{ cm}^{-1}$, $C=N$ (triazole ring) stretching bands at $1578-1633\text{ cm}^{-1}$ and $C=S$ at $1210-1237\text{ cm}^{-1}$. Whereas, aliphatic substituted compounds (12k-n)

were not tautomeric as only singlet corresponds to $-SH$ proton was observed in the region of δ 14.16–14.53 ppm in 1H NMR (supplementary data).

3.2. Biological evaluation

3.2.1. Anti-proliferative investigation against 60 cell lines

All the synthesized compounds were submitted to National Cancer Institute (NCI), Germantown, MD, USA for their anti-proliferative activity against 60 cancer cell lines under nine different cancer cell types (leukemia, lung, colon, CNS, melanoma, ovarian, renal, prostate and breast cancers) with their sub-panels. All these compounds were selected for single concentration of $10\text{ }\mu\text{M}$ and their growth percent data

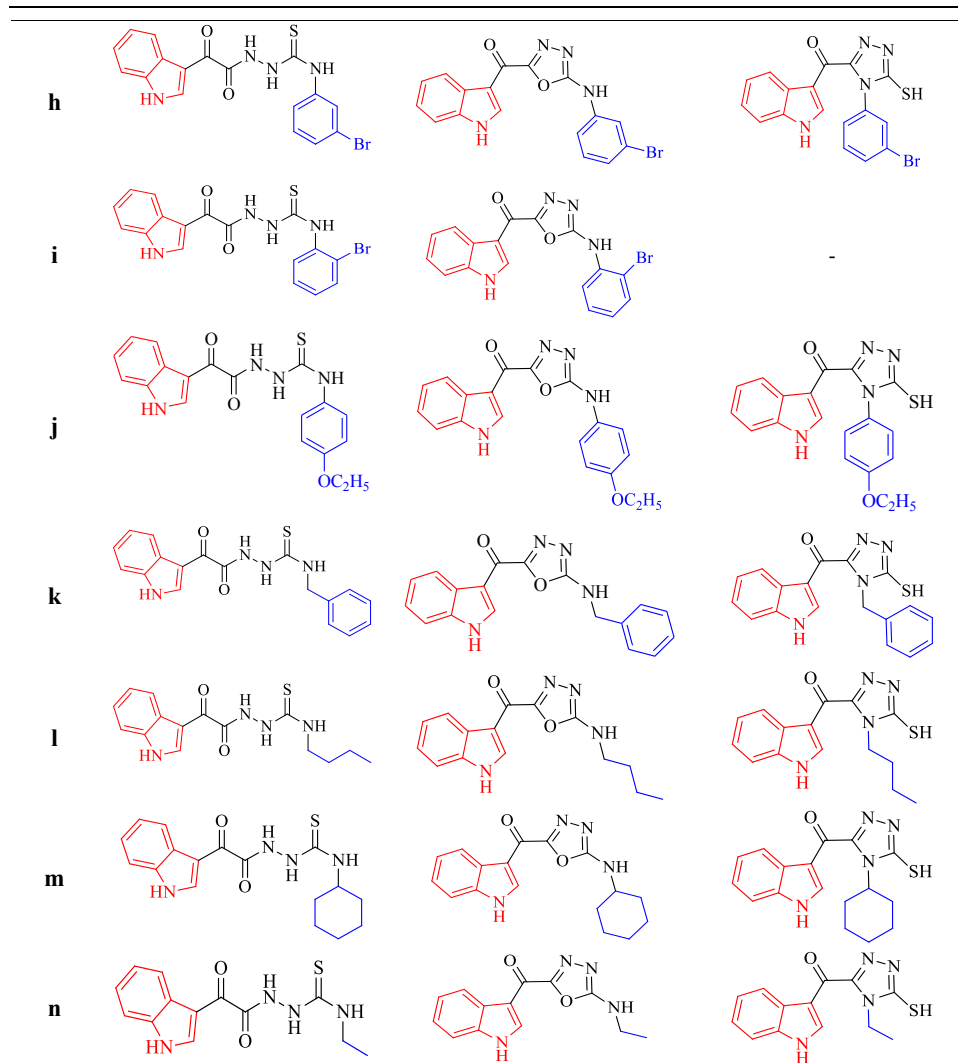
Table 1

Synthesized indole linked 1,3,4-oxadiazole analogues (11a-n) and 1,2,4-triazole (12a, c, e, g, h, j-n).

Code	Thiosemicarbazide (10)	Indole linked 1,3,4-Oxadiazole (11)	Indole linked 1,2,4-triazole (12)
a			
b			-
c			
d			-
e			
f			-
g			

(continued on next page)

Table 1 (continued)



was demonstrated in Tables 2 and 3. Among the 1,3,4-oxadiazole based compounds (11a-n), compounds 11a, 11d, 11e, 11f, 11g and 11k demonstrated considerable anti-proliferative activity against most of the cancer cell lines. Among all, compound 11d showed potent activity against non small lung NCI-H460, colon HCC-2998, Melanoma SK-MEL-5, UACC-62 and breast MCF-7 cancer cell line with % growth of only 19.72–28.16 as shown in Table 2. It also exhibited moderate activity against colon HCT-116 and renal ACHN cancer cell line with 46.71% growth and 37.98% growth respectively (in Table 2). Compound 11a, 11f, and 11g displayed moderate activity against colon HCC-2998 with 37.57–48.72% growth whereas compound 11a, 11d and 11f exhibited good to moderate activity of growth % of 31.16–41.13 of colon KM12 cancer cell line. Compound 11a, 11f, 11g and 11k showed good to moderate activity against breast MCF-7 cancer cell line with % growth of 31.64–47.61 whereas compound 11a, 11d, 11e, 11f, 11g and 11k demonstrated moderate anti-cancer activity against breast T-47D cancer cell line. Compound 11a, 11g and 11f also exhibited moderate activity with 50.60% growth against leukemia HL-60 (TB), 45.01% growth of colon HCC-299 and 45.54% growth of melanoma UACC-62 respectively.

Among all the 60 cancer cell lines, MCF-7 & T-47D cell lines of breast cancer and HCC-2998, HCT-15 & KM 12 cell lines of colon cancer were found to be more susceptible for these classes of compounds.

Among the 1,2,4-triazole based compounds (12a, c, e, g, h, j-n), compounds 12e and 12h were found to be best when compared to other compounds. These compounds exhibited good to moderate activity with 33–50% growth of colon HCC-2998, colon HCT-15, colon KM 12, breast T-47D and breast MCF-7 cancer cell lines as illustrated in Table 3. Compound 12e and 12h was found to be potent against breast T-47D cancer cell line with % growth of 25.26% and 26.08% respectively. Herein, Compound 12e also demonstrated good anti-proliferative activity with % growth of 34.23% against Melanoma SK-MEL-5 cancer cell line. While compound 12h also illustrated moderate activity with % growth of 51.87% against Melanoma UACC-62 cancer cell line. Compound 12a and 12g showed moderate activity against breast T-47D cancer cell line with % growth of 40.36 and 43.78% respectively.

After over viewing the obtained NCI anti-proliferative data from both the series, it has observed that most of the synthesized compounds displayed anti-proliferative activity against melanoma, colon and breast cancer. Compounds 11a, 11d, 11f, 12e, and 12h, showing better activity were taken for further studies.

3.2.2. IC₅₀ value against MCF-7 cancer cell line

From all the synthesized compounds 11a-n and (12a, c, e, g, h, j-n), compounds 11a, 11d, 11f, 12e, and 12h, exhibited 21.88–37.13% of growth of MCF-7 breast cancer cell line according to obtained NCI anti-

Table 2
Anti-proliferative activity of synthesized indole linked 1,3,4-oxadiazole analogues (**11a-n**) against NCI panel of 60 human cancer cell lines.

Cell line/panel	Growth percent													
	11a	11b	11c	11d	11e	11f	11g	11h	11i	11j	11k	11l	11m	11n
Leukemia														
CCRF-CEM	95.07	102.86	87.44	100.34	104.02	94.63	91.15	97.43	97.53	98.20	95.58	107.32	97.61	87.40
HL-60(TB)	50.60	91.79	87.08	72.56	101	100.36	81.34	102.13	102.71	94.02	101.20	104.27		
K-562	101.20	98.67	94.31	107.02	111.70	104.24	98.48	104.74	112.01	109.48	112.81	104.15	91.12	91.12
MOLT-4	92.72	102.85	99.27	103.55	107.93	100.40	107.01	98.19	106.08	103.79	104.74	107.78	87.04	102.07
RPMI-8226	90.01	97.62	91.15	80.01	102.47	90.11	92.01	101.90	93.62	97.89	96.18	103.65	105.13	94.65
SR	86.20	98.78	90.28	79.47	116.09	91.69	95.03	99.55	102.62	106.39	95.46	106.18	70.12	82.55
Non-small cell lung cancer														
A549/ATCC	94.54	101.08	98.10	62.78	95.94	80.31	88.62	92.71	88.21	88.96	84.81	99.87	99.40	106
EKVX	74.19	93.49	97.45	86.34	98.11	85.73	98	98.38	104.45	109.3	97.15	113.25	103.96	79.38
HOP-62	76.32	90.52	90.56	67.15	77.20	70.63	84.68	79.60	79.18	97.73	68.64	84.29	106.46	88.69
HOP-92	78.43	82.08	88.96	97.02	96.76	99.93	84.60	100.55	97.89	97.46	105.11	104.66	106.72	92.66
NCI-H226	77.97	81.91	97.99	84.15	89.72	85.58	84.05	85.20	85.56	88.09	93.40	93.86	93.44	90.06
NCI-H23	87.60	84.73	97.72	65.08	90.27	82.90	88.36	91.30	88.13	89.99	88.58	89.73	96.15	88.59
NCI-H322M	69.71	83.85	92.95	85.42	100.96	86.74	98.81	86.55	94.58	107.20	90.57	104.19	93.92	87.21
NCI-H460	91.13	95.11	104.52	28.16	101.27	56.77	100.21	100.73	99.17	99.77	70.11	107.50	106.73	104.13
NCI-H522	95.24	103.93	100.95	70.60	102.91	79.24	99.53	101.13	98.15	101.61	87.57	91.86	81.25	91.43
Colon cancer														
COLO 205	97.62	108.09	103.62	105.32	107.64	94.72	94.09	102.28	98.86	102.94	102.25	112.99	110.76	107.06
HCC-2998	48.72	85.01	91.48	26.21	54	37.57	45.01	74.74	88.64	98.17	72.63	92.82	98.45	96.83
HCT-116	81.76	78.31	89.80	46.71	93.03	76.68	91.39	96.66	88.38	88.45	87.46	90.82	107.62	91.38
HCT-15	49.77	86.10	98.02	56.70	79.24	64.94	64.06	66.96	80.09	105.99	65.63	101.41	89.80	97.49
HT29	104.20	100.78	102.93	91.30	101.41	109.73	92.98	105.77	100.39	103.81	108.04	103.41	101.37	105.56
KM12	41.13	81.84	91.40	31.16	57.35	37.98	53.76	72.73	81.68	97.33	55.42	81.82	67.75	91.39
SW-620	103.80	95.33	103.79	99.24	99.07	101.59	100.76	100.84	98.73	103.75	101.35	100.08	107.45	101.55
CNS cancer														
SF-268	92.97	89.87	105.88	98.33	102.66	104.22	97.71	102.23	104.79	102.84	105.93	94.49	101.07	100.83
SF-295	101.37	112.75	103.58	103.36	107.13	107.41	106.04	106.60	107.59	108.17	107.98	108.54	111.44	98.03
SF-539	102.34	100.46	105.93	101.41	112.88	110.54	107.33	106.27	103.53	109.6	112.85	109.35	110.52	92.31
SNB-19	94.29	101.80	97.62	103.48	105.30	98.02	103.78	95.98	96.82	103.52	100.48	104.95	103.57	108.02
SNB-75	85.85	98.51	92.45	89.58	87.10	94.16	100.86	89.53	89.25	97.69	98.94	95.39	112.79	91.00
U251	101.86	101.37	96.73	100.33	94.73	97.04	100.35	94.67	96.91	96.59	98.62	99.43	104.52	103.81
Melanoma														
LOX IMVI	90.27	94.32	99.23	99.50	101.21	96.23	97.40	96.75	96.02	102.62	99.68	98.78	100.13	100.04
MALME-3M	101.45	92.60	109.56	111.73	104.91	100.04	102.01	96.85	105.17	109.94	102.90	102.86	95.38	96.27
M15	93.20	99.79	100.59	98.15	104.84	100	95.87	98.57	92.49	96.64	96.69	104.95	121.64	92.92
MDA-MB-435	104.86	111.34	108.10	101.91	103.27	103.77	111.67	103.43	100.50	110.02	107.73	111.04	105.81	105.97
SK-MEL-2	91.16	87.86	99.71	88.29	95.45	92.09	105.33	102.93	110.16	98.08	86.59	90.37	99.57	100.28
SK-MEL-28	107.31	115.64	115.69	104.02	110.67	106.26	107.67	106.22	104.26	110.30	98.49	113.45	111.07	111.33
SK-MEL-5	77.37	88.21	98.66	21.32	88.61	54.80	79.78	78.96	89.45	95.44	71.45	97.96	103.76	100.53
UACC-257	97.91	103.85	96.34	79.05	100.93	89.06	87.73	89.58	92.61	83.16	91.73	107.77	104.03	112.24
UACC-62	65.61	90.68	89.77	19.72	90.54	45.54	82.48	64.16	83	92.15	76	93.26	95.98	94.05
Ovarian cancer														
IGROV1	60.15	62.59	96.31	66.60	79.93	65.58	74.07	70.05	72.62	89.71	80.37	93.22	103.08	85.62
OVCAR-3	89.66	95.11	110.08	83.57	102.70	94.25	95.15	92.33	97.17	105.80	104.34	100.68	103.65	95.38
OVCAR-4	76.63	100.03	92.55	89.42	99.50	99.56	111.74	94.68	105.99	110.47	98.30	108.71	99.29	90.87
OVCAR-5	87.93	119.53	109.43	77.39	85.82	91.64	82.31	86	99.55	111.09	87.50	112.17	105.76	93.75
OVCAR-8	97.59	94.72	99.99	95.42	102.07	93.85	96.41	97.60	94.91	96.51	99.59	105.21	102.63	101.65
NCI/ADR-RES	97.96	95.51	101.92	98.68	104.72	105.02	101.11	101.45	101.70	99.37	115.13	98.39	95.40	101.18
SK-OV-3	87.63	93.06	90.71	82.38	77.33	68.99	79.42	71.52	83.04	89.83	75.30	88.4	105.64	87.35
Renal cancer														
786-0	106.97	98.22	96.43	105.10	104.82	109.71	108.34	107.59	103.07	105.99	103.50	104.04	108.77	97.88
ACHN	85.72	100.98	100.82	37.98	106.60	77.05	97.03	95.74	90.80	102.66	99.59	105.40	108.59	89.71
CAK-1	83.89	96.71	97.25	68.86	93.17	92.52	100.78	93.12	87.43	103.08	98.02	96.48	100.61	87.90
RXF 393	115.68	105.01	110.92	106.37	111.59	109.85	108.75	116.10	124.81	105.32	111.24	111.61	107.60	127.03
SN 12C	98.74	100.66	101.66	94.15	100.08	97.78	96.89	99.92	93.45	97.58	101.54	96.47	98.56	108.57
TK-10	101.48	135.42	117.43	72.87	106.99	96.61	94.98	113.56	112.38	113.25	94.29	118.77	98.56	117.18
UO-31	63.60	78.69	93.77	90.49	98.15	89.70	88.82	92.83	86.97	96.07	93.20	91.26	85.61	71.89
Prostate cancer														
P-C-3	77.22	85.07	87.91	80.01	97.80	89.55	86.45	85.87	87.59	94.10	89.38	94.46	99.62	85.08
DU-155	108.71	96.49	116.37	97.66	112.68	110.88	109.50	106.88	107.04	106.84	112.13	106.84	106.67	109
Breast cancer														
MCF7	31.64	74.86	73.33	21.88	59.10	33.69	47.61	84.53	77.21	77.70	31.92	90.93	67.70	79.72
MDA-MB-231/ATCC	79.40	88.31	100.28	66.74	89.23	75.34	93.78	79.94	88.94	105.63	83.55	92.81	111.46	90.07
HS 578T	98.17	98.62	108.83	89.94	97.11	101.28	105.01	98.60	104.32	101.44	98.24	98.49	97.28	98.97
BT-549	104.07	115.77	108.06	88.70	106.41	101.10	106.58	101.68	103.40	113.07	98.57	107.55	116.56	93.18
T-47D	42.37	71.96	68.41	39.84	43.24	39.87	41.97	67.87	79.56	82.42	38.45	63.30	67.60	64.70
MDA-MB-468	103.49	102.17	98.82	87.94	86.68	91.88	86.34	103.26	103.33	93.55	85.07	103.31	107.45	111.35
Mean GP	86.68	95.88	98.38	87.94	96.00	87.58	92.08	94.13	96.01	100.14	92.20	100.46	99.84	96.18

Table 3
Anti-proliferative activity of synthesized indole linked 1,2,4-triazole analogues (**12a, c, e, g, h, j-n**) against NCI panel of 60 human cancer cell lines.

Cell line/panel	Growth percent									
	12a	12c	12e	12g	12h	12j	12k	12l	12m	12n
Leukemia										
CCRF-CEM	85.06	96.90	88.63	92.02	90.63	83.11	92.52	91.33	94.49	93.26
HL-60(TB)	61.41	83.83	78.12	68.91	88.79	97.20	84.40	90.85	89.29	88.31
K-562	83.33	84.88	86.45	94.74	84.57	88.45	75.07	76.12	87.54	88.77
MOLT-4	85.96	87.73	88.94	83.15	90.19	103.06	96.86	102.71	92.82	93.43
RPMI-8226	68.41	80.97	79.06	91.02	84.09	80.08	81.06	78.67	84.23	69.25
SR	92.01	97.17	86.32	97.61	76.77	96.19	84.30	91.67	86.51	97.11
Non-small cell lung cancer										
A549/ATCC	80.99	98.61	88.03	93.95	86.47	91.46	88.82	92.25	89.15	82.02
EKVX	94.60	94.77	78.20	90.60	70.94	98.45	98.50	90.25	100.06	75.32
HOP-62	87.40	86.59	84.54	90.22	81.73	94.95	98.70	85.99	87.27	71.88
HOP-92	80.33	76.55	89.51	91.97	84.25	79.64	99.50	89.43	86.04	75.10
NCI-H226	77.83	84.15	84.79	90.01	83.08	92.34	96.46	92.51	96.60	70.59
NCI-H23	91.84	100.19	96.05	94.16	87.20	100.30	99.46	92.63	97.40	80.03
NCI-H322M	94.66	102.35	88.90	100.26	77.68	98.41	99.42	96.71	93.98	94.36
NCI-H460	95.67	98.66	100.47	102.63	75	101.50	98.18	98.69	99.18	96.37
NCI-H522	84.66	83.89	84.74	75.02	79.98	90.31	94.45	83.27	87.60	81.63
Colon cancer										
COLO 205	96.82	101.49	109.94	104.24	98.99	107.97	107.63	106.24	73.84	101.91
HCC-2998	58.50	99.84	39.45	81.79	38.77	110.86	100.96	101.48	104.70	98.91
HCT-116	90.26	89.73	89.42	100	89.72	98.88	91.06	92.39	92.54	97.99
HCT-15	64.75	73.65	41.72	63.68	40.88	100.79	95.68	99.04	98.80	104.94
HT29	98.62	94.57	100.98	89.47	96.22	98.31	104.79	99.76	89.88	94.68
KM12	67.38	78.16	49.96	65.95	50.69	88.55	91.11	92.25	83.93	91.43
SW-620	99.95	96.59	93.71	107.41	94.56	96.50	101.03	101.25	96.44	101.20
CNS cancer										
SF-268	95.37	97.87	97.52	95.47	95.41	92.60	97.30	96.92	89.69	93.75
SF-295	103.52	102.12	101.25	96.95	101.55	103.80	90.50	102.55	99.41	102.32
SF-539	94.10	107.67	107.23	109.16	105.99	107.34	98.06	101.70	108.56	96.20
SNB-19	116.18	89.03	100.98	94.10	93.78	92.99	90.43	100.40	103.46	115.40
SNB-75	95.37	88.12	95.76	88.48	83.19	86.07	89.05	81.17	83.03	87.05
U251	105.43	104.30	99.06	106.67	97.31	103.70	93.05	100.04	96.44	106.27
Melanoma										
LOX IMVI	100.43	100.44	98.63	96.83	93.21	98.13	94.91	96.36	89.48	96.29
MALME-3M	105.55	104.62	98.67	110.70	95.39	107.35	108.85	111.45	106.92	100.62
M15	95.88	104.54	99.86	103.98	99.29	101.60	88.54	92.42	88.33	100.92
MDA-MB-435	104.39	102.30	107.33	108.53	102.15	101.16	99.56	98.70	97.78	106.17
SK-MEL-2	86.37	100.37	86.70	89.18	85.88	105.94	99.33	91.93	97.06	86.32
SK-MEL-28	107.41	117.24	119.74	120.96	105.40	118.77	111.40	116.82	115.40	116.24
SK-MEL-5	88.31	89.97	34.23	84.66	27.98	98.41	105.02	99.91	100.30	87.25
UACC-257	99	101.79	90.91	102.96	97.41	98.71	123.47	94.83	89.22	93.72
UACC-62	93.09	81.94	78.28	87.29	51.87	91.81	92.43	81.70	82.83	96.56
Ovarian cancer										
IGROV1	73.10	77.31	71.97	75.74	60.57	90.68	100.05	87.70	93.72	63.45
OVCAR-3	95.25	92.68	91.23	99.38	86.41	97.82	108.13	106.47	96.44	92.39
OVCAR-4	85.01	84.10	92.75	103.02	87.12	84.37	100.62	92.43	92.89	94.20
OVCAR-5	100.67	106.57	96.29	12.83	89.71	118.21	115.65	133.13	115.32	124.07
OVCAR-8	97.13	97.17	97.06	97.79	93.46	98.41	95.47	93.13	94.55	96.10
NCI/ADR-RES	106.05	104.36	101.18	102.95	105.52	98.71	108.56	106.60	101.29	103.89
SK-OV-3	95.44	84.07	83.27	89.01	91.78	91.81	96.67	88.42	89.90	90.38
Renal cancer										
786-0	115.27	103.85	105.22	107.71	103.37	100.24	97.81	101.95	102.83	102.89
A498	87.87	107.21	92.82	108.10	117.92	97.53	100.82	92.05	107.25	97.06
ACHN	96.08	102.97	105.66	113.77	100.30	112.05	100.27	101.51	99.62	97.58
CAK-1	85.39	84.07	80.03	89.33	77.25	87.52	80.51	79.33	73.24	80.81
RXF 393	101.52	102.54	101.64	106.52	104.42	115.97	99.82	107.40	120.96	105.88
SN 12C	92.79	110.65	108.03	113	96.25	98.40	93.97	90.05	100.80	94.55
TK-10	116.96	125.22	115.18	115.58	106.12	134.46	97.61	132.04	122.78	118.22
UO-31	75.19	89.47	86.62	81.60	86.64	86.29	86.46	90.12	88.71	75.98
Prostate cancer										
PC-3	83.87	115.44	86.77	99.73	87.84	89.15	96.56	93.83	94	85.64
DU-155	108.91	66.13	95.40	106.09	103.45	101.88	101.33	103.74	104.99	102.26
Breast cancer										
MCF7	63.32	66.13	37.13	54.78	33.39	85.38	85.91	73.18	84.77	76.35
MDA-MB-231/ATCC	91.33	89.01	86.35	97.70	76.89	96.10	105.74	96.41	89.31	87.94
HS 578T	92.83	95.68	97.42	100.02	93.76	99.0	92.45	90.97	86.18	97.87
BT-549	116.68	112.50	120.43	115.16	119.9	111.78	113.71	115.19	122.84	122.95
T-47D	40.36	50.91	25.26	43.78	26.08	83.01	76.83	77.54	82.22	70.04

(continued on next page)

Table 3 (continued)

Cell line/panel	Growth percent									
	12a	12c	12e	12g	12h	12j	12k	12l	12m	12n
MDA-MB-468	105.90	97.43	92.23	96.95	98.67	102.22	100.30	109.29	106.81	99.89
Mean GP	90.96	94.56	88.54	95.05	85.56	98.08	96.97	96.23	95.52	93.57

Table 4

IC₅₀ profile for compound 11a, 11d, 11f, 12e, 12h, with doxorubicin (standard) and Combretastatin A-4 (standard) against MCF-7 cancer cell line.

	11a (μM)	11d (μM)	11f (μM)	12e (μM)	12h (μM)	Doxorubicin (μM)	CA-4 (nM)
IC ₅₀	5.98	2.42	8.11	3.06	3.30	6.31	2.16

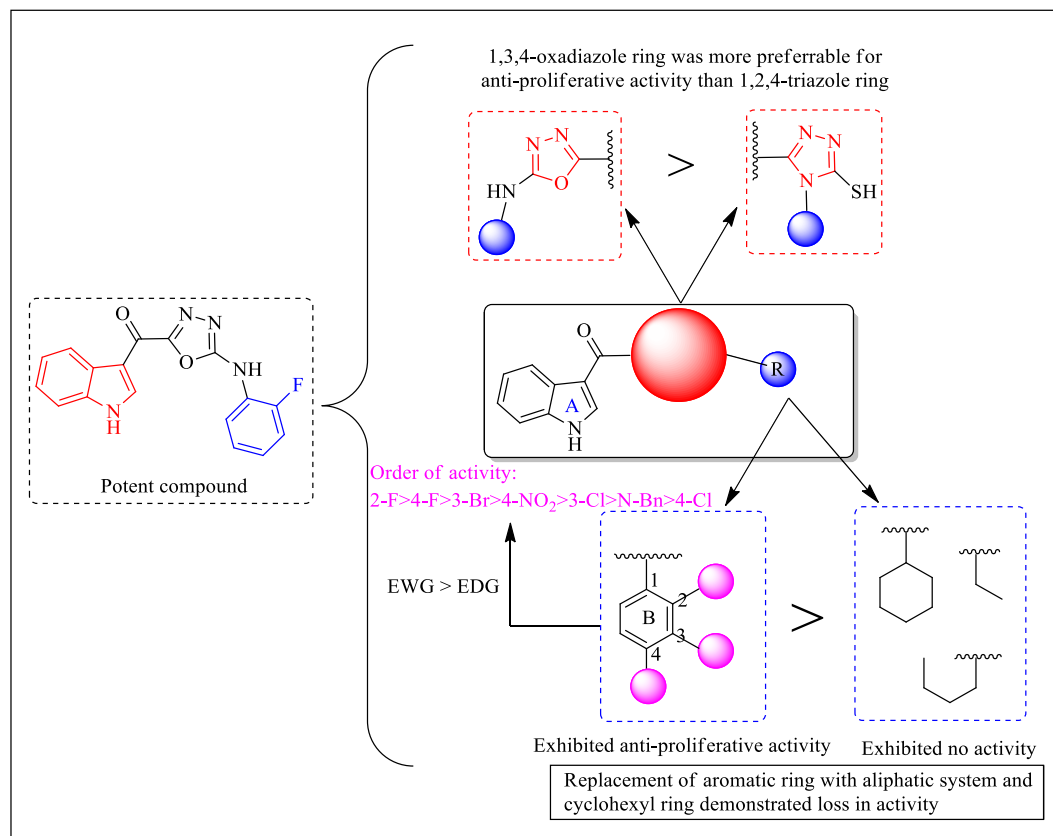


Fig. 3. Structure Activity Relationship for synthesized analogues.

proliferative data. These compounds were screened to evaluate their IC₅₀ values against MCF-7 by MTT (3-(4,5-dimethylthiazol-2-yl)-2,5-diphenyltetrazolium bromide) cytotoxicity assay. Doxorubicin (considered in many chemotherapy regimens, particularly found effective in treatment of breast cancer) and combretastatin A-4 (CBSIs) were used as standard. IC₅₀ values for compound 11a, 11d, 11f, 12e, and 12h, were calculated by dose response curve (supplementary data) and shown in Table 4. Among all the selected compounds, compound 11d demonstrated best cytotoxicity with IC₅₀ 2.42 μM when compared with standard doxorubicin (IC₅₀ 6.31 μM). While, compounds 11a, 12e and 12h, also exhibited good cytotoxicity against MCF-7 breast cancer cell line with IC₅₀ 5.98 μM, 3.06 μM, and 3.30 μM and respectively in comparison to doxorubicin. Compound 11f displayed moderate anti-cancer activity with IC₅₀ 8.11 μM than doxorubicin.

3.2.3. Structure activity relationship

Structure activity relationship has been drawn on the basis of following three parameters (i) Nature of the heterocyclic moiety

attached to indolyl ring; (ii) Nature of the group attached to –NH/–N–; (iii) Nature of the substituents on the aromatic ring.

Analogues with 1,3,4-oxadiazole moiety showed good activity when compared to analogues with 1,2,4-triazole moiety. So, the preferences for anti-proliferative activity of the five membered heterocyclic rings is oxadiazole > triazole. With respect to nature of the substituent's attached to 1,3,4-oxadiazole and 1,2,4-triazole ring, it has been seen that aryl substitution on both the rings (11a, 11d, 11e, 11f, 11g, 12a, 12d, 12e, 12g) showed superior anti-proliferative activity than the aliphatic substitution (11i, 11m, 11n, 12l, 12m, 12n). When both the heterocyclic moieties substituted with aliphatic groups they result in the loss of activity. However when 1,3,4-oxadiazole moiety substituted with benzyl group (11k), it retained the activity and exhibited good anti-proliferative activity against breast cancer cells (MCF-7 with 31.92% growth and T-47D with 38.45%) whereas compound 12k (analogues with 1,2,4-triazole ring attached to benzyl substitution) had no anti-proliferative property.

Nature and positioning of the functional group on aromatic group

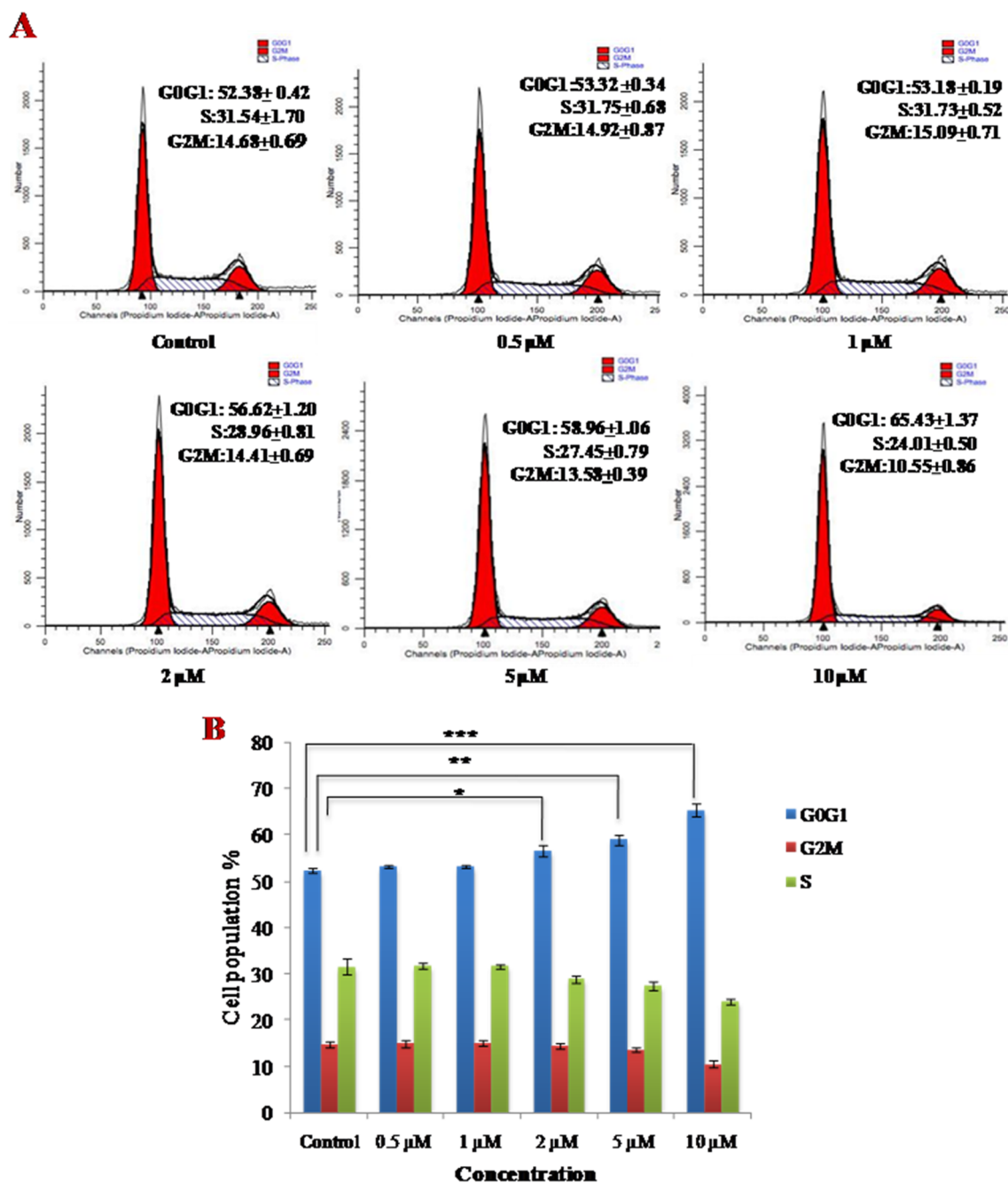


Fig. 4. Compound **11d** induced cell arrest at G0/G1 phase in MCF-7 Cells. (A) 5 and 10 μM concentration of **11d** was incubated with MCF-7 cells for 48 h. Population of cells in different phases of cell cycle were analyzed by Modit LT software and obtained result was shown in histogram. (B) Bar graph showing percentage of cells in different phases of cell cycle. Data are represented as mean \pm SD of separate independent experiments, where (*) indicated $P < 0.05$ and (**) indicated $P < 0.01$ compared to vehicle control as determined by t -test.

greatly influence the activity. Electron withdrawing groups on aromatic ring displayed better activity compared to electron donating groups. Among the electron withdrawing groups halogens have enhanced the activity remarkably. The activity profiles of the substituent's was observed as $\text{F} > \text{Br} > \text{NO}_2 > \text{Cl}$. whereas aromatic substitution of the fluorine atom displayed promising anti-proliferative activity among all the synthesized compounds. On the basis of the positioning of the substituent on aromatic ring, *ortho*- and *para*- substitution was found to be preferable for the activity as shown in Fig. 3.

Among the compounds tested, it has seen compound **11d** (*o*-fluoro) illustrated the best anti-proliferative activity. Compound **11d** emerged as a lead out of the small library of compound screened and was selected for further biological studies.

3.2.4. Cell cycle analysis

Among all the potent anti-proliferative compounds, compound **11d** exhibited best IC_{50} value (2.42 μM) against MCF-7 cell line than that of standard doxorubicin. Thus compound **11d** was selected to examine its effect on progression of cell cycle on MCF-7 cell line.

Distribution profile in different phases of cell cycle was determined by flow cytometry. The results depicted in Fig. 4(A) showed that there was increase of cells in G0/G1 phase from 52.38 ± 0.42 to 65.43 ± 1.37 in dose depended manner (at concentration of 0.5 μM , 1 μM , 2 μM , 5 μM and 10 μM). The percentages of cells in different phases of cell cycle were represented in Fig. 4(B). Compound **11d** provoked cell cycle arrest in G0/G1 phase of cell cycle in MCF-7 cell line at concentration of 10 μM ($p < 0.05$).

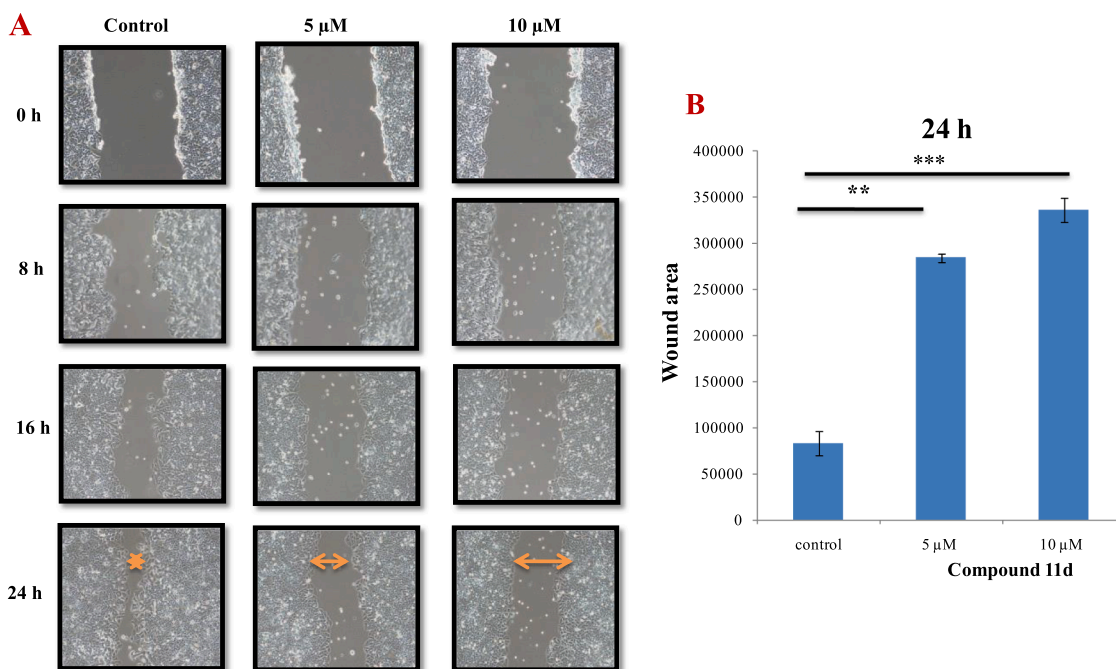


Fig. 5. Effects of **11d** on the migrating ability of MCF-7 cells. (A) MCF-7 cells were grown on 6 wells plate until monolayer was formed, following which a scratch was made and cells were treated with 5 and 10 μM of **11d** and photographs were taken at indicated time points (0,8,16 and 24 h). (B) A significant difference in arbitrary unit analyzed by J software as shown in graph. Data are represented as mean \pm SD, where (**) indicated $P < 0.01$ and (***) indicated $P < 0.001$ compared to vehicle control as determined by t -test.

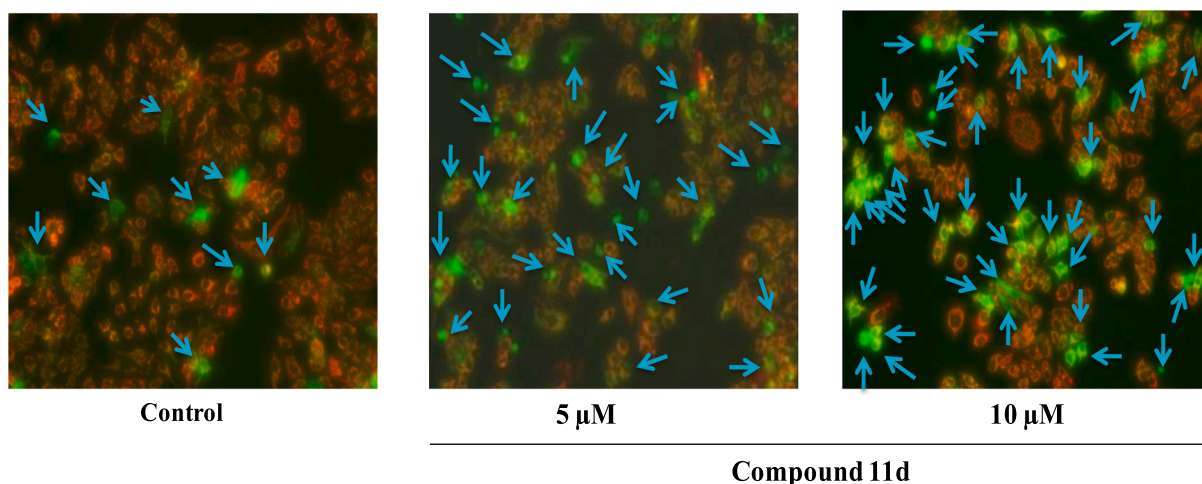


Fig. 6. Effect of **11d** on the mitochondrial membrane potential: MCF-7 cells were treated with 5 and 10 μM and changes in mitochondrial membrane potential were determined by staining with JC-1 dye. Cells undergoing apoptosis and with compromised mitochondrial membrane potential emits green fluorescence whereas cells with polarized potential emit red fluorescence as evident from the photographs.

Table 5
IC₅₀ values for the tested compounds against tubulin polymerization.

	Standard (NOC)	11d	12e
IC ₅₀ (μM)	2.49	3.89	8.32

Generally it has observed that microtubule disrupting agents arrest cell cycle at G₂/M phase but various other studies are reported that microtubules disrupting agents can also induced cell arrest at G₁ phase by altering various gene products *i.e* p53, pRb, p16^{INK4A}, or p21^{waf1/Cip1}, which are involved in cell division at G₁-S phase [24]. Charlie et al. in 2002 reported that disrupted microtubules can also cause cell arrest during interphase at G₁ *via* over expression of p21^{waf1} (p21), a

cyclin-dependent kinases (cdk) inhibitor by monitoring p21^{waf1}-Chk1-cdc25C-cdc2-checkpoint-pathway. Oncogene induced over expression of p21^{waf1} which produced opposite effects on that of Chk1-cdc25C-cdc2 pathway and enhanced cell arrest at G₁ phase [25]. Along with this, Marc *et al* in 1996 also reported that taxol induces cell arrest at late-G₁ in transformed and non-transformed REF-52 and WI-38 mammalian fibroblast cells which is characterized by partially dephosphorylated pRb, and inactive cdk2 kinase (cyclin-dependent kinases) [26]. Here in, Zoe et al. in 1999, determined effect of the MTIs (Microtubule inhibitors), Taxol and vincristine, on the cell cycle kinetics using two isogenic cell lines, HCT116 p21^{+/+} and HCT116 p21^{-/-}. It was examined that p21-deficient cells illustrated dose-dependent, enhanced chemosensitivity to MTIs and these MTIs induced arrest at G₁ [27].

Table 6
Docking score of synthesized compounds (**11a-n**) and (**12a, c, e, g, h, j-n**) for tubulin binding site.

S. No.	Code	Docking score (kcal/mol)	Code	Docking score (kcal/mol)
1	11a	-5.08	12a	-6.16
2	11b	-5.90	12b	-
3	11c	-6.48	12c	-6.43
4	11d	-6.28	12d	-
5	11e	-5.77	12e	-6.66
6	11f	-6.44	12f	-
7	11g	-6.23	12g	-6.60
8	11h	-6.38	12h	-6.28
9	11i	-5.63	12i	-
10	11k	-3.59	12j	-6.44
11	11j	-6.10	12k	-6.73
12	11l	-5.40	12l	-5.77
13	11m	-5.71	12m	-5.17
15	11n	-4.89	12n	-3.79
16	Nocodazole	-5.18	Nocodazole	-5.18

Above studies revealed that MTIs in tumor cells may also caused cell arrest at G₁-S *via* involvement of various gene products.

3.2.5. Cell migration analysis

Among various others anti-cancer effects exhibited by microtubules interacting agents. Interference with cell migration was one of the parameter which has been also reported. So, compound **11d** was evaluated for cell migration by wound healing assay on MCF-7 cell line. The migration potential of compound **11d** was evaluated at 0 h, 8 h, 16 h and 24 h.

As depicted in Fig. 5(A), Cell free area was significantly higher in treated cell as compared to control with passage of time which indicated potential anti-migratory effect of compound **11d**. Thus compound **11d** inhibited the migration of MCF-7 cells in dose dependent manner. The graphical representation of significant difference in the wound area shown by **11d** with respect to control was demonstrated in Fig. 5(B).

3.2.6. Mitochondrial membrane potential (MMP) analysis

Change in the mitochondrial membrane potential is one of the early and prominent features of cells undergoing apoptosis. So, to evaluate whether **11d** induced apoptosis was involved in damaging the integrity of mitochondrial membrane. MMP of **11d** was conducted using a cationic dye JC-1 by fluorescence microscopy on MCF-7 cells. When these cells were treated with 5 μ M and 10 μ M of **11d**, there was increase in green fluorescence in the cytoplasm as dose dependent manner. This characterized that JC-1 monomers when treated with 10 μ M of **11d**, there was more accumulated of the dye in the cytoplasm of cells than the monomer treated with 5 μ M due to compromised MMP. On the other hand, control cells having negative and intact MMP allowed cationic JC-1 dye to enter mitochondria and formed aggregates which were illustrated by red fluorescence in the cytoplasm as shown in Fig. 6. Hence microscopic images were suggesting that **11d** perturbed mitochondrial membrane potential (MMP) of MCF-7 cells in the process of apoptosis.

3.2.7. In vitro tubulin polymerization inhibitory activity

Compounds **11d** and **12e** with best IC₅₀ against MCF-7 cancer cell line were selected for their *in vitro* tubulin polymerization assay and were compared with standard nocodazole. Compounds **11d** and **12e** disturbed the microtubule dynamic by inhibiting polymerization of

tubulin with IC₅₀ 3.89 μ M and 8.32 μ M, whereas the standard nocodazole exhibited IC₅₀ 2.49 μ M against tubulin polymerization as illustrated in Table 5. *In vitro* assay results revealed that **12d** exhibited good tubulin polymerization inhibitory activity than that of **11e** but showed comparative activity to that standard.

3.2.8. Molecular docking study

In silico binding affinities of all the synthesized compounds were determined by using schrodinger software at colchicines binding site of β -tubulin (PDB code 1SA0). Docking score of all the compounds were demonstrated in Table 6. Binding pose of most potent compounds **11d** and **12e** was investigated and compared with standard nocodazole as shown in Fig. 7. Compound **11d** was interacted with VAL 238 amino acid residue through hydrogen bonding with bond length of 2.1 Å. It exhibited hydrophobic interaction with LEU 242, CYS 241, ILE 378, VAL 318, ALA 317, ALA 316, VAL 315, ALA 354, VAL 351, MET 259, LEU 255, LEU 252, ALA 250, LEU 248 amino acid residue and also exhibited other interaction with THR 239, THR 314, LYS 352, ASN 350, ASN 349, ASN 258 amino acids residue of β -tubulin complex. Compound **12e** displayed no hydrogen bond but showed hydrophobic interaction with MET 259, VAL 257, LEU 255, LEU 248, ALA 250, VAL 238, ILE 378, CYS 241, LEU 242, VAL 318, ALA 317, ALA 316, VAL 315, ALA 354 amino acid residues. It also exhibited other kinds of interactions with various residues of β -tubulin complex (ASN 258, LYS 254, THR 239, THR 314, LYS 352, ASN 350). Nocodazole (standard) illustrated hydrogen bonding with ASN 258 and ASN 349 with bond length 2.3 Å and 1.8 Å respectively. It also exhibited hydrophobic interaction with ILE 347, PRO 261, MET 259, LEU 255, LEU 248, CYS 241, ALA 354, VAL 351, ILE 347, VAL 315, ALA 316, ALA 317, VAL 318 amino acid. Nocodazole also demonstrated other interaction with ASN 258, ASN 349, ASN 350, LYS 352, THR 353 and THR 314 amino acid residues as shown in Fig. 7.

Compounds **11d** and **12e** were superimposed with standard drugs nocodazole at colchicine binding site of β -tubulin complex. Benzimidazole ring of nocodazole was superimposed with 2-fluoro phenyl ring of compound **11d** and 4-fluoro phenyl ring of compound **12e** whereas thiophene ring of nocodazole was superimposed with 1,3,4-oxadiazole ring of compound **11d** and carbonyl group of compound **12e** as illustrated in Fig. 7(E,F). Docking score of **11d** (-6.28 kcal/mol) and **12e** (-6.66 kcal/mol) was also better than that of nocodazole (-5.18 kcal/mol) as illustrated in Table 6.

4. Conclusion

A series of twenty four 1,3,4-oxadiazole and 1,2,4-triazole based topoisomerase II inhibitors were synthesized by simple synthetic methodology and evaluated for their anti-proliferative activity. Anti-proliferative screening suggested that compounds **11a**, **11d**, **11f**, **12e**, **12h**, showed good to moderate activity against a panel of various NCI cancer cell lines. Compounds **11d** and **12e** were found to be best compounds from both the series. The most potent Compound **11d** showed good specificity against non-small cell lung cancer (NCI-H460), Colon cancer (HCC-2998, HCT-116, KM12), Melanoma (SK-MEL-5, UAAC-62), Renal (ACHN), and Breast (MCF-7, T-47D) Compound **11d** also demonstrated good anti-proliferative activity against MCF-7 cancer cell line cancer cell line with best IC₅₀ 2.42 μ M. Whereas, compound **12e** and **12h** displayed good IC₅₀ 3.06 μ M and 3.30 μ M against MCF-7 cancer cell line. Further mechanistic studies illustrated that **11d** induced cell arrest at G₀/G₁ phase and also depolarized mitochondria membrane potential of MCF-7 cell line. Wound healing assay revealed that **11d** reduced cell growth by lowering cell migration potential in dose dependent manner.

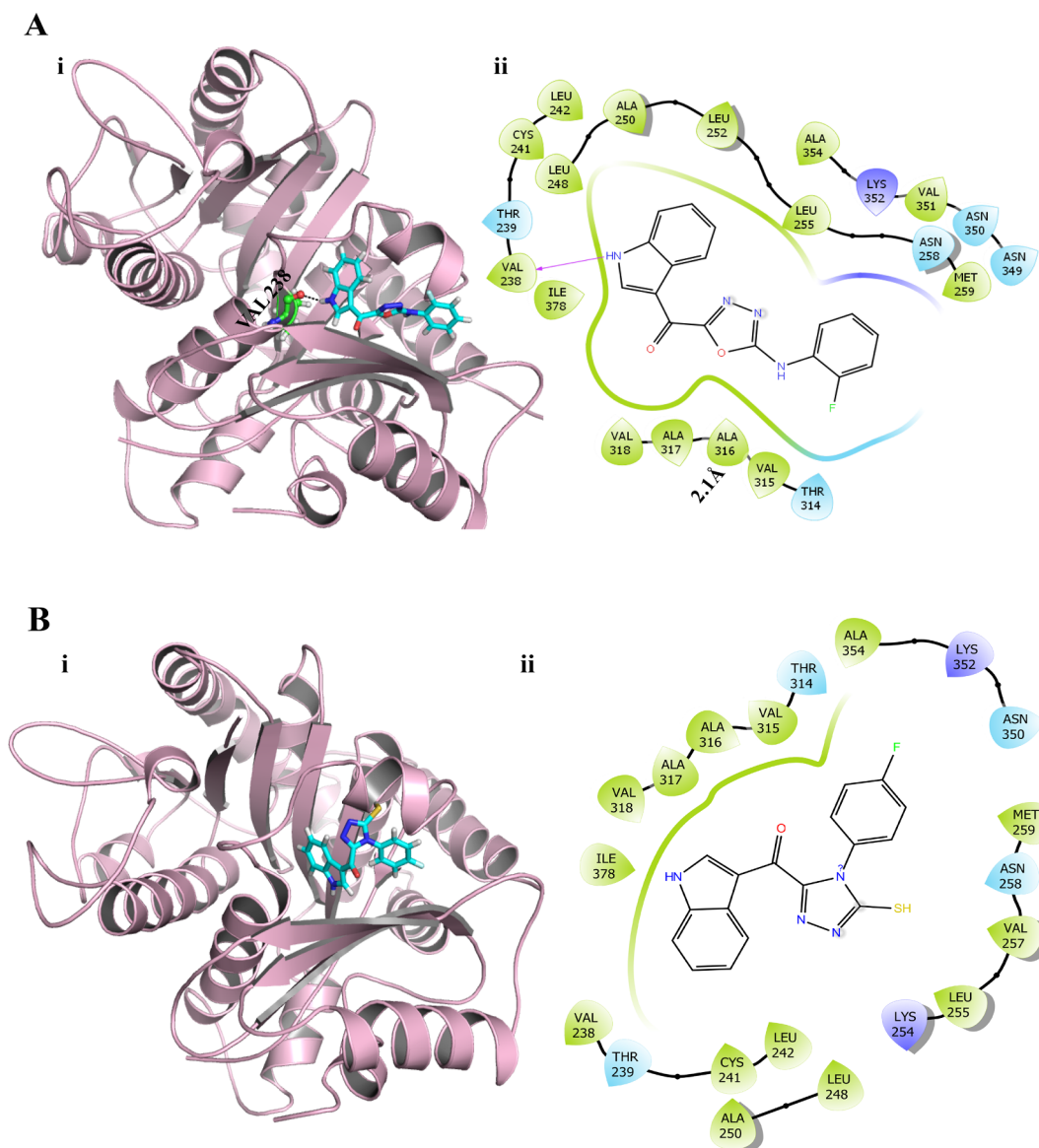


Fig. 7. (A) (i) Binding pose of **11d** (cyan) at colchicine binding site of β -tubulin are shown in stick representation while protein is rendered in cartoon representation and black colour dotted line is depicted hydrogen bonding with VAL 238 residues as ball and stick. (ii) Lig plot of **11d** in the binding pocket of β -tubulin; (B) (i) Binding pose of **12e** (cyan) at colchicine binding site of β -tubulin (PDB code: 1SA0) are shown in stick representation while protein is rendered in cartoon representation (ii) Lig plot of **12e** in the binding pocket of β -tubulin; (C) (i) Binding pose of **nocodazole** (cyan) at colchicine binding site of β -tubulin are shown in stick representation while protein is rendered in cartoon representation and black colour dotted line is depicted hydrogen bonding with ASN 258 and ASN 349 residues as ball and stick. (ii) Lig plot of **nocodazole** in the binding pocket of β -tubulin; (D) Superimposition of docking pose of **11d** (pink) and **12e** (cyan) with **nocodazole** (yellow) at colchicine binding site of β -tubulin.

To find the mode of action for compounds **12e** and **11d** for exhibiting anti-proliferative activity, *In-vitro* polymerization assay was done and indicated that **11d** potently inhibited tubulin polymerization with IC_{50} 3.89 than **12e**. *In silico* molecular docking results showed that compounds **11d** and **12e** were occupying colchicine binding site of β -tubulin with good docking score -6.66 kcal/mol and -6.28 kcal/mol respectively when compared to nocodazole (-5.18 kcal/mol). Further on **11d** will be selected as the lead molecule for further investigation.

Declaration of Competing Interest

The authors declare that they have no known competing financial interests or personal relationships that could have appeared to influence the work reported in this paper.

Acknowledgments

FN would like to express their deep sense of gratitude to Jamia Hamdard for financial support under Jamia Hamdard-Silver Jubilee Research Fellowship-2017 and is also grateful to ICMR, New Delhi for the award of Senior Research Fellowship. We thank Hon'ble Vice Chancellor, Jamia Hamdard for financial assistance under research promotion grant.

Authors are also thankful to Dr. Mohammed Nayel (Project Manager), Developmental Therapeutics Program (DTP), for carrying *in vitro* anti-proliferative activity against a panel of 60 human cancer cell lines at National Cancer Institute, Bethesda, MD, USA.

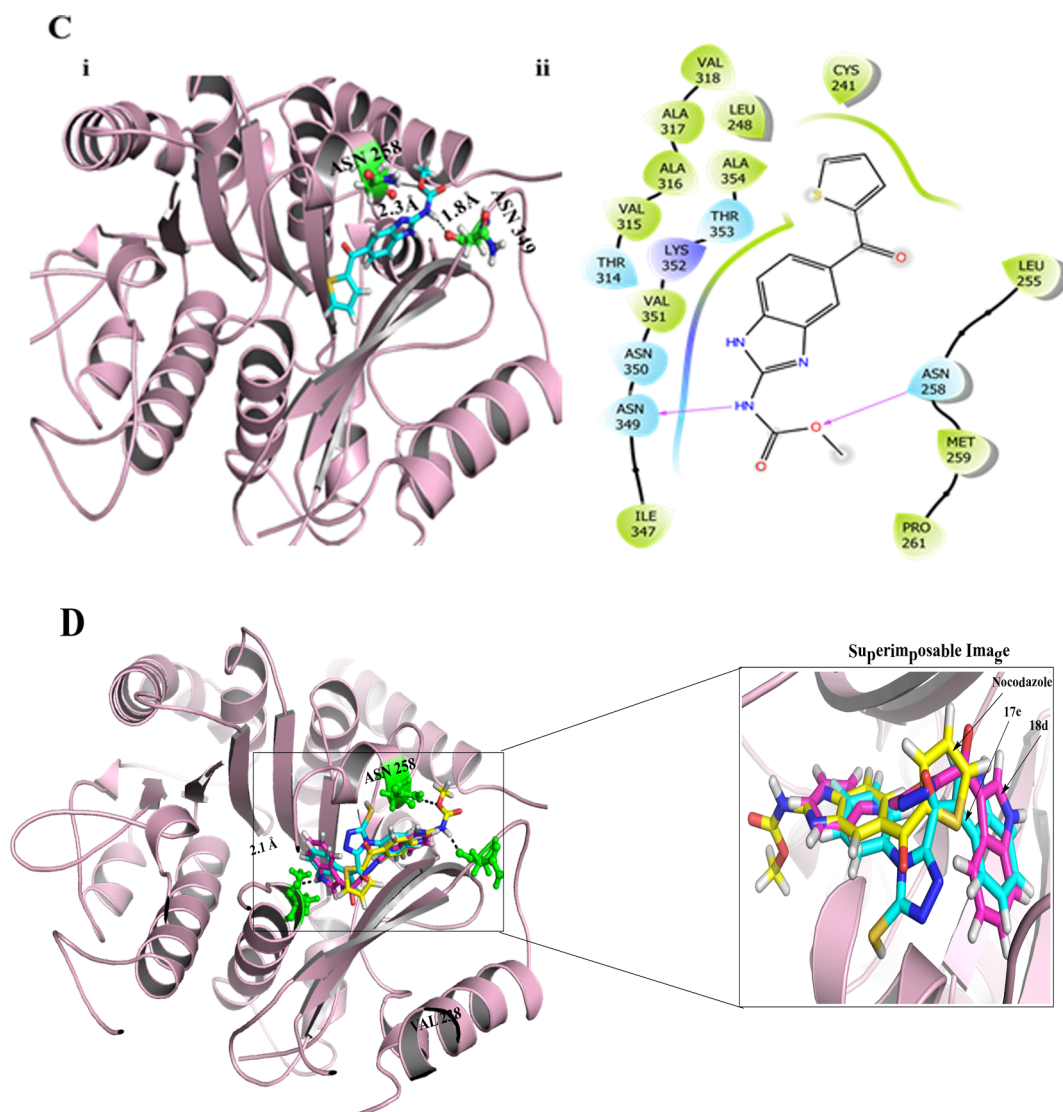


Fig. 7. (continued)

Appendix A. Supplementary material

Supplementary data to this article can be found online at <https://doi.org/10.1016/j.bioorg.2019.103519>.

References

- [1] A. Sudhakar, History of cancer, ancient and modern treatment methods, *J. Cancer Sci. Ther.* 1 (2009) 1–4.
- [2] L.S. Penna, J.A.P. Henriques, D. Bonatto, Anti-mitotic agents: are they emerging molecules for cancer treatment? *Pharmacol. Ther.* 173 (2017) 67–82.
- [3] R. Heald, E. Nogales, Microtubule dynamics, *J. Cell Sci.* 115 (2002) 3.
- [4] E. Mukhtar, V.M. Adhami, H. Mukhtar, Targeting microtubules by natural agents for cancer therapy, *Mol. Cancer Ther.* 13 (2014) 275–284.
- [5] M. Emanuela, C. Giuseppe, C. Sonia, E. Cellupica, S. Pantalone, P. Francesca, R. Marta, S. Angela Marika, S. Collina, Vinca alkaloids and analogues as anti-cancer agents: looking back, peering ahead, 2018.
- [6] Y.N. Cao, L.L. Zheng, D. Wang, X.X. Liang, F. Gao, X.L. Zhou, Recent advances in microtubule-stabilizing agents, *Eur. J. Med. Chem.* 143 (2018) 806–828.
- [7] Y. Lu, J. Chen, M. Xiao, W. Li, D.D. Miller, An overview of tubulin inhibitors that interact with the colchicine binding site, *Pharm. Res.* 29 (2012) 2943–2971.
- [8] Q. Zhang, Y. Peng, X.I. Wang, S.M. Keenan, S. Arora, W.J. Welsh, Highly potent triazole-based tubulin polymerization inhibitors, *J. Med. Chem.* 50 (2007) 749–754.
- [9] S. Dadashpour, S. Emami, Indole in the target-based design of anticancer agents: a versatile scaffold with diverse mechanisms, *Eur. J. Med. Chem.* 150 (2018) 9–29.
- [10] P.H.B. França, D.P. Barbosa, D.L. da Silva, É.A.N. Ribeiro, A.E.G. Santana, B.V.O. Santos, J.M. Barbosa-Filho, J.S.S. Quintans, R.S.S. Barreto, L.J. Quintans-Júnior, J.X. de Araújo-Júnior, Indole alkaloids from marine sources as potential leads against infectious diseases, *Biomed. Res. Int.* 2014 (2014) 375423–375423.
- [11] S. Tsujii, K.L. Rinehart, S.P. Gunasekera, Y. Kashman, S.S. Cross, M.S. Lui, S.A. Pomponi, M.C. Diaz, Toposentin, bromotoposentin, and dihydrodeoxy-bromotoposentin: antiviral and antitumor bis(indolyl)imidazoles from Caribbean deep-sea sponges of the family Halichondriidae. Structural and synthetic studies, *J. Org. Chem.* 53 (1988) 5446–5453.
- [12] M. Kumar, K.K. Vijaylaxmi, A. Pal, Anti-inflammatory and antioxidant properties of Spongosorites halichondriodes, a marine sponge, 2014.
- [13] N.S. Burres, D.A. Barber, S.P. Gunasekera, L.L. Shen, J.J. Clement, Antitumor activity and biochemical effects of toposentin, *Biochem. Pharmacol.* 42 (1991) 745–751.
- [14] A. Carbone, V. Spano, B. Parrino, C. Ciancimino, O.A. Attanasi, G. Favi, A facile synthesis of deaza-analogues of the bisindole marine alkaloid toposentin, *Molecules (Basel, Switzerland)* 18 (2013) 2518–2527.
- [15] V. Janganani, J. Ponder, S. Thakkar, C.T. Jordan, P.A. Crooks, Succinamide derivatives of melampomagnolide B and their anti-cancer activities, *Bioorg. Med. Chem.* 25 (2017) 3694–3705.
- [16] S.R. Pedada, N.S. Yarla, P.J. Tambade, B.L. Dhananjaya, A. Bishayee, K.M. Arunasree, G.H. Philip, G. Dharmapuri, G. Aliev, S. Putta, G. Rangaiiah, Synthesis of new secretory phospholipase A2-inhibitory indole containing isoxazole derivatives as anti-inflammatory and anticancer agents, *Eur. J. Med. Chem.* 112 (2016) 289–297.
- [17] M. Mustafa, D. Abdelhamid, E.M.N. Abdelhafez, M.A.A. Ibrahim, A.M. Gamal-Eldeen, O.M. Aly, Synthesis, antiproliferative, anti-tubulin activity, and docking study of new 1,2,4-triazoles as potential combretastatin analogues, *Eur. J. Med. Chem.* 141 (2017) 293–305.
- [18] W. Li, Y. Yin, W. Shuai, F. Xu, H. Yao, J. Liu, K. Cheng, J. Xu, Z. Zhu, S. Xu, Discovery of novel quinazolines as potential anti-tubulin agents occupying three zones of colchicine domain, *Bioorg. Chem.* 83 (2018) 380–390.
- [19] S. Sakamuru, M.S. Attene-Ramos, M. Xia, Mitochondrial membrane potential assay, *Meth. Mol. Biol. (Clifton, N.J.)* 1473 (2016) 17–22.

- [20] F. Naaz, M.C. Preeti Pallavi, S. Shafi, N. Mulakayala, M. Shahar Yar, H.M. Sampath Kumar, 1,2,3-triazole tethered Indole-3-glyoxamide derivatives as multiple inhibitors of 5-LOX, COX-2 & tubulin: their anti-proliferative & anti-inflammatory activity, *Bioorg. Chem.* 81 (2018) 1–20.
- [21] V. Patel, A. Singh, D. Jain, P. Patel, R. Veerasamy, P.C. Sharma, H. Rajak, Combretastatin A-4 based thiophene derivatives as antitumor agent: development of structure activity correlation model using 3D-QSAR, pharmacophore and docking studies, 2017.
- [22] H. Cai, X. Huang, S. Xu, H. Shen, P. Zhang, Y. Huang, J. Jiang, Y. Sun, B. Jiang, X. Wu, H. Yao, J. Xu, Discovery of novel hybrids of diaryl-1,2,4-triazoles and caffeic acid as dual inhibitors of cyclooxygenase-2 and 5-lipoxygenase for cancer therapy, *Eur. J. Med. Chem.* 108 (2016) 89–103.
- [23] F.Y. Miyake, K. Yakushijin, D.A. Horne, A concise synthesis of topoisomerase II inhibitors nortopoisomerase II B and D, *Org. Lett.* 2 (2000) 2121–2123.
- [24] P. Giannakakou, R. Robey, T. Fojo, M.V. Blagosklonny, Low concentrations of paclitaxel induce cell type-dependent p53, p21 and G1/G2 arrest instead of mitotic arrest: molecular determinants of paclitaxel-induced cytotoxicity, *Oncogene* 20 (2001) 3806–3813.
- [25] C.R. Mantel, V.M. Gelfano, Y.J. Kim, A. McDaniel, Y. Lee, H.S. Boswell, H.E. Broxmeyer, P21waf-1-Chk1 pathway monitors G1 phase microtubule integrity and is crucial for restriction point transition, *Cell Cycle (Georgetown, Tex.)* 1 (2002) 327–336.
- [26] M.O. Trielli, P.R. Andreassen, F.B. Lacroix, R.L. Margolis, Differential Taxol-dependent arrest of transformed and nontransformed cells in the G1 phase of the cell cycle, and specific-related mortality of transformed cells, *J. Cell Biol.* 135 (1996) 689–700.
- [27] Z.A. Stewart, D. Mays, J.A. Pietsenpol, Defective G₁-S cell cycle checkpoint function sensitizes cells to microtubule inhibitor-induced apoptosis, *Cancer Res.* 59 (1999) 3831.